# The long non-coding RNA *MaTAR20* promotes mammary tumor growth by regulating angiogenesis pathways

Sarah D. Diermeier[1,2,*], Kung-Chi Chang[2,3], Ashleigh Frewen[1], Padraig Taaffe[1], Joke C. Grans[1], Haoyu Xiong[1], Brian A. Benz[2], Suzanne Russo[2], Dawid Nowak[2], Stephen Hearn[2], Allen Yu[2,4], John E. Wilkinson[5], Frank Rigo[6], and David L. Spector[2,3,4*]

[1]Department of Biochemistry, University of Otago, Dunedin 9016, New Zealand
[2]Cold Spring Harbor Laboratory, Cold Spring Harbor, NY 11724, USA
[3]Stony Brook University, Molecular and Cellular Biology Program, Stony Brook, NY 11794, USA
[4]Stony Brook University, Genetics Program, Stony Brook, NY 11794, USA
[5]Department of Pathology, University of Michigan, Ann Arbor, MI 48109, USA
[6]Ionis Pharmaceuticals, Carlsbad, CA 92010, USA

[*]Correspondence:
Sarah D. Diermeier (sarah.diermeier@otago.ac.nz, +64 20 4221985) or
David L. Spector (spector@cshl.edu, +1 (516) 367-8456)

**Running title:** *MaTAR20* as new driver of mammary tumor growth

**Keywords:** long non-coding RNAs; breast cancer; antisense oligonucleotides; Vegf; Tnfsf15

**Financial Support:**

This research was supported by NCI 5P01CA013106-Project 3 (D.L.S.), CSHL/Northwell Health support (D.L.S), a Susan G. Komen postdoctoral fellowship (S.D.D.), NCI 1K99CA215362-01 (S.D.D), RDF-UOO1802 awarded by the Royal Society Te Apārangi (S.D.D.), the New Zealand Cancer Society (S.D.D.) and the Breast Cancer Foundation New Zealand (S.D.D.).

**Conflict of interest:**

The authors declare no conflict of interest. D.L.S. is a consultant to, and receives research reagents from, Ionis Pharmaceuticals.

**Abstract**

Long non-coding RNAs (lncRNAs) are an emerging class of regulatory molecules that have been shown to play important roles in tumorigenesis and cancer progression. Here, we studied the recently identified lncRNA *Mammary Tumor Associated RNA 20* (*MaTAR20*) in mammary cancer progression. A CRISPR/Cas9 knockout of *MaTAR20* in the metastatic 4T1 cell line led to reduced cancer cell proliferation and increased cell surface adhesion compared to control cells. Consistent with these knockout results antisense oligonucleotide (ASO) mediated knockdown of *MaTAR20* resulted in reduced growth and invasion in 4T1 cells, and in primary mammary tumor organoids derived from the MMTV-PyMT mouse model of breast cancer. Injection of *MaTAR20*-specific ASOs subcutaneously into tumor bearing MMTV-PyMT mice resulted in smaller and highly necrotic tumors in comparison to mice injected with a scrambled control ASO. To investigate the molecular mechanism by which *MaTAR20* acts to advance mammary tumor progression, we applied a combination of RNA-sequencing and RNA-pulldown coupled to DNA-sequencing. These analyses demonstrated that the nuclear retained lncRNA is associated with several essential cancer signaling pathways such as VEGF signaling. In particular, *MaTAR20* directly binds to and regulates the expression of *Tnfsf15*. Our results indicate that *MaTAR20* is an important driver of mammary tumor progression and represents a promising new therapeutic target.

56 **Introduction**

57 Breast cancer (BC) is estimated to account for 30% of new cancer diagnoses and
58 15% of cancer-related deaths in women in 2021 (1). While currently available chemo- and
59 targeted therapies have led to improved overall survival rates, declines of mortality have
60 slowed over the past decade compared to other types of cancer (1). Metastatic disease
61 in particular is the main cause for BC related mortality (1), indicating the need for
62 innovative approaches to target the metastatic cascade.

63 Recent studies highlight the potential of long non-coding RNAs (lncRNAs) as new
64 therapeutic targets in cancer (2-13). Many lncRNAs are expressed in a tissue- and
65 cancer-specific manner (14,15) and several previous studies have supported a role for
66 lncRNAs as drivers of tumorigenesis, tumor growth and invasion (reviewed in (16) and
67 (17)). A promising new approach of targeting lncRNAs to reduce mammary tumor growth
68 and metastasis *in vivo* are nucleic acid based therapies (reviewed in (17)). Initial success
69 in targeting oncogenic lncRNAs was shown using locked nucleic acids (LNAs) to target
70 *BCAR4* (5) or antisense oligonucleotides (ASOs) for *Malat1* (6,18).

71 We previously identified 30 *Mammary Tumor Associated RNAs* (*MaTARs*) (7).
72 These lncRNAs are over-expressed in mouse models of BC and in human breast tumor
73 tissue compared to normal mammary epithelial cells (7). ASO-mediated knockdown of
74 various *MaTARs* in primary mammary tumor cells resulted in a tumor cell - specific
75 reduction of cell growth (7). Recently, we demonstrated that *MaTAR25* expression
76 contributes to BC progression via regulation of the *Tensin1* gene (13). Here, we
77 investigated the potential of *MaTAR20* (also known as *Gm13387*, *RP23-132N23.1*,
78 *ENSMUSG00000087028*) as a new therapeutic target in BC, as well as the molecular

79 mechanism by which *MaTAR20* acts. ASO-mediated knockdown or CRISPR/Cas9
80 knockout of *MaTAR20* results in reduced cell proliferation and migration. Further, ASO
81 knockdown of *MaTAR20 in vivo* leads to delayed tumor onset, decreased tumor size,
82 increased tumor necrosis and reduced metastatic burden. To further study the potential
83 of this lncRNAs as a therapeutic target, we generated two loss-of-function and one gain-
84 of-function models of the human orthologue, *hMaTAR20*. Our *in vitro* and *in vivo*
85 characterization of these models suggest that the lncRNA is indeed a new driver of breast
86 cancer cell proliferation and migration. Based on our investigation of the molecular
87 mechanism of *MaTAR20* function, the observed phenotype is likely the result of reduced
88 tumor vascularization upon reduction in the level of *MaTAR20*. *MaTAR20* regulates genes
89 involved in tumor angiogenesis, such as increasing the expression of the *Vascular*
90 *Endothelial Growth Factor A and B* (*Vegf-A*, *Vegf-B*) genes and it directly binds to the
91 *Tnfsf15* locus to repress its expression during tumor progression.
92

93 **Materials and Methods**

94 **Murine cell culture**

95 Murine 4T1, Py2T, G0771 and D2A cells were cultured in DMEM supplemented
96 with 10% FBS and 1% penicillin/streptomycin. All cells were grown in a cell culture
97 incubator at 37 °C and 5% CO2. ASOs were delivered to the cells via free uptake
98 immediately after seeding the cells. For proliferation assays, cells were seeded in 24-well
99 plates and trypsinized at individual time points. Cell counts were determined manually
100 using a hemocytometer. Cell cycle analysis was performed using a BrdU FITC kit (BD)
101 as described (13).

102 **Organoid culture**

103 Murine mammary tumor organoids were generated and cultured as previously
104 described (7,19). Briefly, organoids were generated from nulliparous MMTV-PyMT
105 tumors, mixed with growth factor-reduced Matrigel and grown in DMEM/F12 medium
106 supplemented with 1x ITS (insulin, transferrin, and sodium selenite), 1%
107 penicillin/streptomycin and murine FGF2 (2.5 nM). For ASO-mediated knockdown
108 experiments, organoids were seeded at a density of 5 organoids/µl and plated as 80 µl
109 domes in 24-well dishes. ASOs were added directly (free uptake) to the culture medium
110 15-20 min after the organoids were plated and in fresh medium at day 3. Organoids were
111 incubated for a total of 6 days. ASO sequences are provided in Supplementary Table S1.
112 For visualization purposes and quantification of organoid branching, images were
113 acquired using an Axio-Observer Live Cell inverted microscope (Zeiss).

114 **Scanning electron microscopy (SEM)**

115 SEM on 2D cells was performed as described previously (20). Briefly, cells cultured
116 on glass coverslips were fixed in 1.6% glutaraldehyde in PBS for 30 minutes and then
117 dehydrated in a graded ethanol series. Coverslips were critical point dried (CPD) using a
118 Samidri 795 CPD device (Tousimis), mounted on aluminum stubs with carbon tabs
119 (Electron Microscopy Sciences). Samples were coated with gold using an Emitech K550X
120 Sputter Coater. Samples were imaged with a Hitachi S3500 SEM operated at 5 kV.

121 For SEM of 3D organoids, Matrigel containing organoid samples were removed
122 from multi-well tissue culture dishes (using a 3.5 mL disposable transfer pipette and
123 placed in 45 mL of cold PBS (4°C) in 50 mL capacity polypropylene centrifuge tubes
124 (VWR Scientific). Matrigel was washed away by 3-4 rounds of suspension in cold PBS

125 and centrifugation using a refrigerated centrifuge set to 1,000 pm, 20 min, 4°C (Beckman
126 Coulter Allegra X15r). After the final wash to remove Matrigel, organoids were transferred
127 to 1.6 mL microcentrifuge tubes and fixed in 1% glutaraldehyde in PBS at 4°C, for 30
128 minutes, rinsed in distilled water by centrifugation and resuspension and then post-fixed
129 in 1% aqueous osmium tetroxide (Electron Microscopy Sciences) for 30 minutes at RT.
130 After osmium fixation, organoids became dense relative to solutions and a centrifuge was
131 not needed for further handling. Organoids were dehydrated in a graded ethanol series
132 and then immersed in 50% hexamethyldisilazane (HMDS, Electron Microscopy Sciences)
133 in 100% ethanol for 5 min and 100% HMDS for 10 min. Organoids in 0.3 mL of HMDS
134 were aspirated using a transfer pipette and the solution and suspended organoids were
135 deposited to 12 mm diameter SEM stubs coated with carbon adhesive tabs (Ted Pella
136 Inc) and allowed to air dry. Samples were coated with gold using an Emitech K550X
137 Sputter Coater and imaged with a Hitachi S3500 SEM operated at 5 kV.

138 **RNA extraction and qRT-PCR**

139 Total RNA was isolated from cells or organoids using TRIzol. DNase I treatment
140 was performed for 15 min at RT to remove contaminating DNA. cDNA synthesis was
141 carried out using the TaqMan Reverse Transcription kit (Life Technologies) and random
142 hexamers according to the manufacturer's instructions. Quantitative Real time PCR (qRT-
143 PCR) was performed using the Power SYBR Green Master Mix (Life Technologies).
144 Cycling conditions were as follows: 15 min at 95 °C followed by 40 cycles of 15 sec at 94
145 °C, 30 sec at 60°C. *Peptidylprolyl isomerase B* (*cyclophilin B*) was used as an
146 endogenous control in mouse and *RPL13* in human to normalize each sample and
147 relative expression results were calculated using the $2^{-\Delta\Delta Ct}$ method. A list of primers used

148 is provided in Supplementary Table S1.

149 **Subcellular localization**

150 For single-molecule FISH, cells were seeded onto acid-washed glass coverslips
151 and fixed in 4% paraformaldehyde when reaching 50% confluency. RNA-FISH was
152 carried out using the Affymetrix View ISH Cell Assay Kit and custom probes (Thermo
153 Fisher) according to the manufacturer's instructions. For human tissue, Pantomics
154 BRC481 tissue microarrays were used. The slides were imaged on a LSM 710/780
155 confocal microscope (Zeiss). Cell fractionation assays were performed as described in
156 (13).

157 **CRISPR/Cas promoter deletion**

158 To generate a genetic knockout, two sgRNAs targeting the promoter region were
159 combined, creating a deletion. A sgRNA targeting the *Renilla* luciferase gene was used
160 as non-targeting control. All sgRNAs were cloned into a lentiCRISPR_V2 plasmid
161 (Addgene #52961) also encoding Cas9 and delivered to the cells using lentiviral
162 transduction as described (21). Stable integrants were selected using puromycin
163 selection and single cell sorted using a FACS Aria (SORP) Cell Sorter. Each single cell
164 clone was propagated and analyzed by genomic PCR and qRT-PCR to select for
165 homozygous knockout clones. Sequences for sgRNAs are provided in Supplementary
166 Table S1.

167 **Invasion assay**

168 Invasion assays were performed as described previously in (7). Briefly, a Cultrex®
169 96 well BME Cell Invasion Assay (Trevigen) was used. Cells were starved in FBS-free
170 culture medium, then harvested and seeded at a density of 5 x $10^4$ cells/well into the

171 invasion chamber. ASOs were added to growth medium containing 10% FBS. The plate
172 was incubated at 37 °C for 24 h and the assay was performed according to the
173 manufacturer's instructions. The fluorescence was measured with a SpectraMax i3 Multi-
174 Mode Detection Platform (Molecular Devices) using the 480/520 nm filter set. Each
175 sample was measured in triplicate.

176 **Rescue Assay**

177 *MaTAR20* isoforms were amplified by PCR using Phusion High-Fidelity DNA
178 Polymerase (NEB) following the manufacturer's instructions. *MaTAR20* isoform 1 was
179 cloned using XhoI and EcoRI-HF overhangs. The digested PCR product was ligated into
180 a pCMV6-Entry plasmid (Origene) with T4 DNA ligase. Isoforms 2 and 3 were amplified
181 by PCR, gel extracted and treated with T4 PNK. The pCMV6-Entry plasmid was digested
182 using EcoRV-HF and Eco53kI followed by dephosphorylation using Quick CIP. Isoforms
183 2 and 3 were ligated into the pCMV6-Entry backbone as described above. Ligations were
184 transformed into competent DH5α cells using heat shock. Transformants were selected
185 for using Kanamycin at 25 µg/mL and validated using Sanger sequencing.

186 For ectopic expression of *MaTAR20*, knockout cells were seeded into 96-well
187 plates at a density of 5,000 cells/well. The plates were incubated overnight (16-18 h) at
188 37 °C with 5% CO2. DNA was transfected using Lipofectamine 2000 (Thermo Fisher) in
189 serum-free DMEM medium at a ratio of 100 ng DNA : 0.2 µL Lipofectamine. After 6 h, the
190 medium was replaced with 100 µL/well of fresh complete medium. Cells were fixed for
191 each time point using 100 µL/well of staining solution (150 µg/mL saponin, 4 µg/mL DAPI,
192 0.5% PFA in PBS) for 30 minutes with gentle shaking at RT, then stored at 4 °C .The cells
193 were counted using a Cytation5 automated cell counting system.

194 RNA was isolated 24 h after transfection. The medium was removed and 50 µL of
195 TRIzol was added to each well of a 96-well plate. RNA was extracted according to the
196 manufacturer's instructions. For each sample, 1 µg of RNA was treated with ezDNase
197 and reverse transcribed to cDNA using SuperScript IV VILO following the manufacturer's
198 instructions (Thermo Fisher). For RT-qPCR testing of the *MaTAR20* rescue, PowerUp
199 SYBR Green Master Mix (Thermo Fisher) was used. All RT-qPCRs were run on a
200 QuantStudioTM 3 Real-Time PCR Machine (Applied Biosystems).

201 ***hMaTAR20* CRISPR/Cas9 knockout cell lines**

202 T47D cells were cultured in RPMI-1640 medium supplemented with 10% FBS, 0.2
203 Unit/mL human insulin and 1% penicillin/streptomycin. A sgRNA targeting the mouse
204 *MaTAR20* gene was used as non-targeting control (M888). All sgRNAs were cloned into
205 a lentiCRISPR_V2 plasmid (Addgene #52961) also encoding Cas9 and delivered to the
206 cells using lentiviral transduction as described (21). Stable integrants were selected using
207 puromycin selection and single cell sorted using a FACS Aria (SORP) Cell Sorter. Each
208 single cell clone was propagated and analyzed by genomic PCR and qRT-PCR to select
209 for homozygous knockout clones (19bp deletion; hg38 chr9:137295224-137295246).

210 **CRISPRi**

211 MDA-MB231-LM2 (LM2) cells (22) were cultured in DMEM supplemented with
212 10% FBS and 1% penicillin/streptomycin. We used lentiviral transduction to integrate
213 dCas9 (pHAGE EF1α dCas9-KRAB, Addgene # 50919) as described (21). A sgRNA
214 targeting the *Renilla* luciferase gene was used as non-targeting control. sgRNAs targeting
215 the promoter region of *hMaTAR20* (hg38 chr9:137295979-137295998 for -277; chr9:
216 137296113-137296128 for -390) were cloned into pLenti SpBsmBI Hygro plasmid

217 (Addgene #62205) and delivered to the MDA-MB231-LM2-dCas9 cells using lentiviral
218 transduction. Stable integrants were selected using hygromycin selection. For *in vivo*
219 experiments 400,000 cells were xenografted into the L4 mammary fat pad of Nu/J mice
220 (n=10 each for *Ren* control and *hMaTAR20* KD cells).

221 **CRISPRa**

222 MCF10A cells were cultured in a media consisting of DMEM/F12 + GlutaMAX +
223 5% Horse Serum + 20 ng/ml EGF + 0.5 mg/ml Hydrocortisone + 100 ng/ml Cholera Toxin
224 + 0.28 Units/ml Insulin. For CRISPR activation (CRISPRa) two plasmids carrying the
225 components of the tagging system SUperNova (SunTag) were integrated into MCF10A
226 cells by lentiviral transduction (23). The utilized plasmids were obtained from Addgene:
227 pHRdSV40-scFv-GCN4-sfGFP-VP64-GB1-NLS (#60904) and pLV-sgCDKN1B#2 BFP
228 (#60903). All sgRNAs were cloned into the plasmid backbone pLenti SpBsmBI Hygro
229 (Addgene #62205), and stable integrants were selected using hygromycin selection.

230 **Proliferation assay**

231 The proliferation assay was performed by DAPI staining of the cell nuclei and
232 automatically counted by a CytationTM 5 Cell Imaging Reader (BioTek). Briefly, cells
233 were trypsinized and counted manually with a hemocytometer. One thousand cells per
234 well were seeded into 10 wells of four 96-well plates. Cells were fixed and stained at 24
235 h, 48 h, 72 h, and 96 h post seeding with 100 µl staining solution (PBS, 150 ng/ml
236 Saponin, 8 ng/ml DAPI, 0,5% PFA) per well for 30 minutes.

237 **Scratch assay**

238 Scratch assays were performed following the protocol according to (24). Cells were
239 trypsinized, seeded into a 24-well plate (or 6-well plates for MCF10A) and grown to full

240 confluence. The cell monolayer was scratched using a 200 μL pipette tip to create a
241 straight wound, followed by washing off floating cells with medium. Images were taken
242 directly after scratching (T0) and after 24 h culturing (T24), and the rate of wound closure
243 was calculated using Image J.

244 **Animal experiments**

245 Animal experiments were carried out in the CSHL Animal Shared Resource, in
246 accordance with IACUC approved procedures. MMTV-PyMT mice (25) were obtained
247 from Dr. Mikala Egeblad (CSHL). Tumors and normal mammary glands were extracted
248 immediately after euthanizing the animal and processed to generate primary cells,
249 organoids or tissue sections. For *in vivo* ASO injections, female MMTV-PyMT mice were
250 divided into two cohorts, being treated either with a *MaTAR20*-specific ASO or a
251 scrambled control ASO at ~8-10 weeks of age (after formation of palpable tumors). MOE
252 ASOs were injected subcutaneously three times per week (n=4 for scASO, n=5 for
253 *MaTAR20* ASO). cET ASOs were injected twice per week, both at 50 mg/kg per dose
254 (n=7 for scASO, n=7 for *MaTAR20* ASO). Tumors were measured twice per week
255 throughout the treatment course. At the end of the experiment, mice were euthanized,
256 and primary tumors and lungs were fixed in 4% PFA and embedded in paraffin for histo-
257 pathological analysis, or snap-frozen for RNA extractions. FFPE blocks were sectioned
258 and stained with hematoxylin and eosin (H&E). Slides were scanned and analyzed using
259 the Aperio ImageScope software. Immunohistochemistry was performed using the
260 following antibodies: Tnfsf15 (Bioss, BS-5092R), Anti-Ki67 (AbCam, ab15580), Cleaved
261 Caspase-3 (Cell Signaling, 9661), VegfB (Invitrogen, PA5-80220), VegfA (AbCam,
262 ab1316). The resulting images were analyzed using QuPath software v0.2.3(26).

263 **RNA-seq**

264 RNA quality was assessed on an Agilent 2100 Bioanalyzer. Libraries were
265 prepared on samples with RIN ≥9 using the Illumina TruSeq sample prep kit v2 and
266 sequenced on an Illumina NextSeq instrument. Data was analyzed as previously
267 described (7). Briefly, the quality of FASTQ files was assessed using FastQC
268 (http://www.bioinformatics.babraham.ac.uk/projects/fastqc/). Reads were mapped to
269 GRCm38 using STAR (27), and the reads per gene record were counted using HTSeq-
270 count (28). Differential gene expression was performed with DESeq2 (29), and an
271 adjusted p-value of < 0.05 was set as threshold for statistical significance. KEGG pathway
272 and GO term enrichment and was carried out using the R/Bioconductor packages GAGE
273 (30) and Pathview (31).

274 **ChIRP-seq**

275 ChIRP-seq was carried out as previously described (13). Briefly, 20 million cells
276 were harvested and fixed in 1% glutaraldehyde solution. ChIRP was performed using two
277 individual tiling pools of biotinylated oligonucleotide probes. A probe pool targeting mouse
278 *Ppib* was used as negative control. A list of ChIRP-seq probes is provided in
279 Supplementary Table S1. ChIRP-Seq libraries were generated using the Illumina TruSeq
280 ChIP Library Preparation Kit and sequenced on an Illumina NextSeq instrument. ChIRP-
281 seq data quality was assessed using FastQC
282 (http://www.bioinformatics.babraham.ac.uk/projects/fastqc/) and paired-end reads were
283 mapped to GRCm38 using Bowtie2 (32). ChIRP-seq analysis was performed using
284 HOMER (33). For RT-qPCRs testing the ChIRP cDNA, 5 ng cDNA and 5 μM of primers
285 in 10 μL was used (reagents and cycling conditions as described under “Rescue assay”).

286 **Data access**

287 RNA-seq and ChIRP-seq data have been deposited at Gene Expression Omnibus

288 (GEO) under accession number GSE171085.

289

290 **Results**

291 ***MaTAR20* is a tumor-specific, nuclear-retained lncRNA**

292 *MaTAR20* is an intergenic lncRNA gene located on mouse chromosome 2.
293 According to GENCODE vM18, three isoforms of the *MaTAR20* transcript exist,
294 comprising 2,646, 659 and 638 nt (Figure 1A). Our computational analysis of ENCODE
295 expression data revealed that the lncRNA is absent or expressed at low levels in normal
296 mammary glands and other normal tissues, but highly expressed (FPKM >200) in
297 mammary tumors derived from the transgenic MMTV-PyMT mouse model of luminal BC
298 (Figure 1B). Furthermore, *MaTAR20* levels correlate with tumor size in the MMTV-PyMT
299 model (Supplementary Figure S1A).

300 To examine the localization of *MaTAR20* we performed single molecule RNA-FISH
301 in primary MMTV-PyMT cells (Figure 1C). Our results indicate that *MaTAR20* is indeed
302 an abundant lncRNA in primary mammary tumor cells, and predominantly localizes to the
303 nucleus, averaging 10-40 foci per nucleus. We further confirmed that *MaTAR20* is a
304 nuclear-retained transcript by subcellular fractionation assays, which revealed an
305 enrichment in both the nucleoplasm and the chromatin fractions (Figure 1D), a localization
306 pattern comparable to the lncRNA *Malat1*. Our initial characterization indicates that
307 *MaTAR20* is a tumor-specific, nuclear-enriched lncRNA that may play a role in tumor
308 progression based on its expression profile.

309 **Knockdown of *MaTAR20* leads to reduced organoid branching**

310 To determine if *MaTAR20* is a driver of mammary tumor cell growth, we performed
311 knockdown experiments *ex vivo*, in MMTV-PyMT derived tumor organoids (6,7,34)
312 (Figure 1E-H). Organoids are an excellent model system to study cancer biology and to

313 test new therapeutic treatments (for review, see (35)). Wildtype/untreated organoids
314 exhibit a branched morphology consistent with collective cell migration (Fig 1G-H) and/or
315 proliferation (for review, see (36). We achieved *MaTAR20* knockdown efficiencies of 50-
316 60% using 2'-O-methoxyethyl (MOE) ASOs in 3D mammary tumor organoids by free
317 uptake (Figure 1E). Treatment of MMTV-PyMT tumor organoids with two independent
318 MOE ASOs targeting *MaTAR20* lead to an up to 40% reduction of organoid branching
319 compared to untreated organoids, or organoids treated with a scrambled control MOE
320 ASO (scASO) (Figure 1F-H). Based on these and our previous results in primary
321 mammary epithelial cells (7), we conclude that *MaTAR20* enhances both the proliferative
322 and migratory potential of mammary tumor cells.

323 **Promoter deletion of *MaTAR20* results in a less aggressive phenotype**

324 To independently validate our ASO-mediated knockdown results, and to develop
325 a model system that enables us to study the molecular mechanism of *MaTAR20* in detail,
326 we generated *MaTAR20* loss-of-function cells using the CRISPR/Cas9 system. First, we
327 tested a panel of mouse mammary tumor cell lines to identify a suitable model system.
328 Of the tested cell lines, the metastatic 4T1 line (37) showed the highest *MaTAR20*
329 expression level (Supplementary Figure S2A). Next, we established promoter deletion of
330 *MaTAR20* by stably integrating Cas9 and two guide RNAs (gRNAs): the first gRNA was
331 designed to bind upstream of the *MaTAR20* transcription start site (at -736) and the
332 second gRNA binding within the first exon of *MaTAR20* (+12 bp) (Figure 2A), resulting in
333 promoter deletion of 748 bp. A gRNA targeting the *Renilla* luciferase gene was used to
334 generate negative control cells. All edited cell populations were single cell sorted to
335 generate monoclonal cell lines. Two *MaTAR20* knockout clones (KO1, KO2) and two

336 negative control clones (Ren1, Ren2) were analyzed further. The KO cell lines showed a
337 ~80-85% reduction of *MaTAR20* expression compared to control clones (Figure 2B). We
338 used four different primer pairs to measure *MaTAR20* levels, one amplifying all three
339 isoforms of *MaTAR20* (PP1, Figure 2B), and three isoform-specific primer pairs (PP2,
340 PP3, PP4; Supplementary Figure S2B). Our results indicate that all three isoforms of
341 *MaTAR20* were reduced to comparable levels in the KO cells.

342 Similar to our ASO-mediated knockdown experiments in primary mammary tumor
343 cells (7), we observed a 30-40% reduction of cell proliferation in the KO cell lines (Figure
344 2C). This phenotype was not caused by differences in cell cycle profiles (Figure 2D) and
345 did not correlate with Cas9 expression (Supplementary Figure S2C). Ectopic expression
346 of *MaTAR20* in KO cells was able to rescue the cell proliferation phenotype, restoring
347 growth rates to levels comparable to Ren control cells (Supplementary Figure S3A-B).
348 This finding also indicates that the *MaTAR20* transcript is responsible for the observed
349 phenotype, rather than the genomic locus itself playing a regulatory role and that
350 *MaTAR20* plays a role in *trans*.

351 While culturing the *MaTAR20* KO cells, we noticed a difference in cell adhesion
352 between the KO clones and the control cell lines. The KO cells were particularly difficult
353 to dislodge from cell culture flasks, leading to increased (2-4 fold) trypsinization times
354 required to detach the KO cells. Further examination of the KO and Ren control cells
355 using scanning electron microscopy revealed that reduced *MaTAR20* levels may lead to
356 stronger surface attachment of the cells, accompanied by more organized, sheet-like
357 structures (Figure 2E). In summary, promoter deletion of *MaTAR20* leads to reduced

358 tumor cell growth and migration compared to control cells, similar to primary cells treated
359 with *MaTAR20* ASOs (Figure 1).

360 **The human orthologue, *hMaTAR20,* drives breast cancer cell growth**

361 We previously identified the human orthologue of *MaTAR20*, *hMaTAR20*, by
362 synteny as *RP13-122B23.8 (ENSG00000260996*), located on chromosome 9 (7). To
363 investigate whether *hMaTAR20* drives breast cancer cell growth and therefore may hold
364 clinical significance, we first performed computational analyses of *hMaTAR20* expression
365 of TCGA data. The lncRNA is overexpressed 2-fold across all subtypes of breast cancer
366 compared to adjacent normal breast tissue, with highest levels in estrogen receptor
367 positive (ER+) breast cancer (Figure 3A). RNA-FISH on a tissue microarray further
368 confirmed a 2-fold up-regulation of *hMaTAR20* in breast cancer compared to
369 corresponding normal tissue (Figure 3B). Further stratifying the breast cancer tissue
370 revealed highest levels of *hMaTAR20* in grade II-III tumors (Supplementary Figure S4A),
371 following a similar trend of increased expression in later stage tumors as observed in
372 mouse (Supplementary Figure S1).

373 We performed an expression screen in several breast cancer cell lines, which
374 further confirmed that ER+ cell lines show increased levels of *hMaTAR20* (Supplementary
375 Figure S4B), with T47D showing the highest levels. Therefore, we generated a
376 CRISPR/Cas9 driven deletion in exon 1 in T47D cells, which resulted in stable reduction
377 of *hMaTAR20* levels (Figure 3C) in two single cell clone derived cell lines (KO C9 and KO
378 V2). Lower *hMaTAR20* levels lead to reduced cell proliferation in T47D KO cells
379 compared to control cells grown in 2D culture and reduced branching in spheroid culture,
380 with more pronounced effects in the 3D assay (Figure 3D-E). We also observed reduced

381 2D migration in *hMaTAR20* KO cells (Figure 3F). Like *MaTAR20* in mouse, *hMaTAR20*
382 showed predominantly nuclear localization (Supplementary Figure S4C), suggesting the
383 lncRNA functions similarly in both organisms.

384 While *hMaTAR20* expression is highest in ER+ breast cancer, the lncRNA is also
385 overexpressed in all other types of breast cancer compared to adjacent normal tissue. To
386 study the impact of *hMaTAR20* in an ER- model, we generated a CRISPR interference
387 (CRISPRi) driven transcriptional repression model of *hMaTAR20* in the aggressive basal
388 cell line MDA-MB-231-LM2 (22)(Supplementary Figure S4D). Similar to the T47D KO
389 cells, we observed reduced cell proliferation, spheroid branching and cell migration in the
390 MDA-MB-231-LM2 CRISPRi model (Supplementary Figure S4E-G).

391 Next, we tested whether increasing *hMaTAR20* levels in the pre-malignant cell line
392 MCF10A may lead to an increase in proliferative and migratory potential. MCF10A cells
393 express *hMaTAR20* at very low levels compared to T47D or MDA-MB-231-LM2 cells
394 (Figure 3B). Using CRISPR activation (CRISPRa), we up-regulated endogenous
395 *hMaTAR20* expression using three different sgRNAs (Figure 3G). We observed increased
396 cell proliferation and viability as well as increased migration compared to control cells
397 (Figure 3H-I). In summary, our results show that *hMaTAR20* is a driver of cell proliferation
398 and migration in human breast cancer cells, recapitulating the phenotype we observed
399 with *MaTAR20* in the mouse system.

400 **cET ASO shows improved knockdown efficiency *in vitro***

401 To determine the effect of *MaTAR20* reduction on tumor progression, and to
402 investigate whether ASOs are a viable strategy to systemically reduce *MaTAR20*, we
403 performed *in vivo* experiments in transgenic mouse models of breast cancer. First, we

404 designed a constrained ethyl (cET) ASO targeting *MaTAR20*. In comparison to MOE
405 ASOs (Figure 1), cET ASOs show increased potency *in vivo* (38) and are the chemistry
406 of choice for tissues less sensitive to ASO modulation with several clinical trials currently
407 ongoing (39).

408 Before introducing the cET ASO into animals, we tested its knockdown (KD)
409 efficiency *in vitro*. Concentrations as low as 250 nM were sufficient to achieve >60%
410 knockdown of *MaTAR20* within 24 h in 4T1 cells (Figure 4A), and we observed KD
411 efficiencies of >95% using 500 nM after 72 h (Figure 4B). These results compare
412 favorably to concentrations of 4-5 μM of MOE ASOs achieving ~50% KD in organoids
413 (Figure 1) and ~70% KD in primary cells (7). Knockdown of *MaTAR20* using the cET ASO
414 resulted in significantly reduced cell proliferation and invasion (Figure 4C-D), however, it
415 is possible that the difference in proliferation impacts on the readout of the invasion assay
416 as well. These results agree with our observations using MOE ASOs (Figure 1) and
417 *MaTAR20* promoter deletions in mouse (Figure 2) as well as our findings for *hMaTAR20*
418 (Figure 3).

419 **Knockdown of *MaTAR20 in vivo* leads to a reduction in tumor growth and induces**
420 **tumor necrosis**

421 To further investigate the potential of cET ASOs targeting *MaTAR20* in mammary
422 tumors, we injected 100 mg/kg/week of either *MaTAR20* cET or a negative control ASO
423 (scrambled = scASO cET) into MMTV-PyMT (C57BL/6) mice after palpable tumor
424 formation (n=7 for scASO, n=8 for *MaTAR20* ASO; Figure 5A). We achieved an 80%
425 reduction of *MaTAR20* in the tumors on average, further highlighting the potency of the
426 cET chemistry (Figure 5B). We initiated ASO injections on animals with comparable

427 average tumor burden in both cohorts and observed a 30% overall reduced tumor burden
428 in *MaTAR20* cET treated mice over the course of eight weeks (Figure 5C). While mice in
429 the *MaTAR20* cET group eventually went on to develop tumors, tumor onset was delayed
430 in comparison to the scASO cET group. Furthermore, when comparing the growth curves
431 of similarly sized tumors that developed at the same time in both cohorts, tumors in the
432 *MaTAR20* cET group grew slower compared to scASO cET treated mice, resulting in a
433 difference of 75% after 8 weeks (Figure 5D). After all mice reached the study endpoint,
434 we carried out hematoxylin and eosin (H&E) staining of the fixed tumors to investigate
435 potential histo-pathological differences. Notably, tumors in the *MaTAR20* cET treated
436 group showed severe necrosis compared to the control group (Figure 5E).

437 To confirm that the human orthologue of *MaTAR20* acts similarly to the mouse
438 lncRNA in an *in vivo* situation, we xenografted one of our loss-of-function models, the
439 modified MDA-MB-231-LM2 cells into the mammary fat pad of nude mice. We observed
440 reduced tumor growth and increased tumor necrosis (Figure 5F-G), further confirming the
441 functional role of the *hMaTAR20* in tumor progression.

442 **Knockdown of *MaTAR20 in vivo* leads to reduced metastatic burden**

443 The MMTV-PyMT model is highly aggressive, with a metastasis incidence rate of
444 >80% (25). We examined the lungs in our *in vivo* study post-mortem for macro-metastatic
445 nodules. While 7/7 mice in the scASO group developed at least one macro-metastatic
446 nodule, only 4/7 mice in the *MaTAR20* ASO cohort presented macro-metastatic lesions
447 (Supplementary Figure S5A). We went on to examine the histo-pathology of the four lungs
448 that developed metastasis by H&E staining and discovered that metastases in the
449 *MaTAR20* ASO treated group showed cystic, differentiated nodules compared to the solid

450 masses detected in the scASO cohort (Supplementary Figure S5B-C). We suggest that
451 metastatic nodules in animals that received the *MaTAR20* cET may have developed prior
452 to treatment start, and that the cystic phenotype is a consequence of systemic *MaTAR20*
453 knockdown, impacting already existing metastases. Alternatively, the observed
454 differences could be due to reduced overall tumor burden.

455 To independently validate our animal studies, we performed a second *in vivo*
456 experiment using *MaTAR20* MOE ASO1 and injected it into MMTV-PyMT (FVB) mice
457 (Supplementary Figure S5D). Similar to the cET experiments in C57/Bl6, we observed
458 reduced tumor growth for the *MaTAR20* ASO group compared to the scASO group from
459 around week 4 of treatment (Supplementary Figure S5E). H&E staining of tumor sections
460 revealed that animals in the *MaTAR20* MOE group also developed more necrotic tumors
461 compared to control animals (Supplementary Figure S5G). In addition, we observed a
462 reduction of macro-metastatic nodules in the lungs of 3/4 mice receiving *MaTAR20* MOE
463 ASO1 (Supplementary Figure S5F), confirming the trend of reduced metastasis upon
464 *MaTAR20* knockdown.

465 Immunohistochemistry staining of the tumor sections for Ki67 revealed slightly
466 reduced levels in both MOE and cET cohorts. We did not observe a consistent trend when
467 staining for the apoptosis marker cleaved caspase 3, indicating that the tumors likely
468 undergo necrosis rather than programmed cell death (Supplementary Figure S6A-B). In
469 summary, our *in vivo* experiments show that systemic reduction of *MaTAR20* using ASOs
470 leads to delayed mammary tumor onset, reduced tumor growth, increased tumor necrosis
471 and reduced metastasis.

472 ***MaTAR20* expression level correlates with VEGF expression**

473 We set out to identify the molecular mechanism by which *MaTAR20* impacts tumor
474 cell growth and invasion. As our RNA-FISH and subcellular fractionation assays indicated
475 that *MaTAR20* is a nuclear-retained lncRNA (Figure 1), we hypothesized that it may act
476 by impacting gene expression. First, we performed a computational co-expression
477 analysis using lncRNA2function (40). Similar approaches have been previously applied
478 successfully to identify the molecular role of other lncRNAs (41). Notably, we observed a
479 strong enrichment for pathways involved in angiogenesis, with the top 7 most enriched
480 pathways being related to vascular endothelial growth factor (VEGF) signaling (Figure
481 6A), including "Signaling by VEGF", "VEGF hypoxia and angiogenesis" and "Sorafenib
482 Pharmacodynamics", a multi-kinase inhibitor that has been shown to act on VEGF
483 receptor (VEGFR) (42). Due to this striking ontology enrichment, we set out to
484 experimentally assess if *MaTAR20* and VEGF expression correlate. We determined by
485 qRT-PCR that Vegf-A and Vegf-B are reduced in tumors of MMTV-PyMT mice that
486 received the *MaTAR20* cET ASO compared to the scASO control group (Figure 6B).
487 Immunohistochemistry staining of tumor sections confirmed this trend on the protein level
488 (Supplementary Figure S6C-D). We also assayed CD31 staining in the tumors to probe
489 for differences in angiogenesis and observed reduced CD31+ cells in *MaTAR20* ASO
490 treated animals (Supplementary Figure S6E), which may point to a reduced number of
491 blood vessels being formed upon *MaTAR20* loss.

492 We used RNA extracted from whole tumors for the qRT-PCR validations described
493 above. While MMTV-PyMT tumors generally contain a high percentage of cancer cells
494 (Figure 5E, Supplementary Figure S5E), qRT-PCR from whole tumors cannot distinguish
495 between expression changes in tumor or stromal cells. To investigate whether VEGF

496 expression was reduced in the same cell type as *MaTAR20*, we measured VEGF
497 expression in 4T1 cells with successful *MaTAR20* KD (Figure 4A/B). Indeed, we observed
498 a 35% reduction of Vegf-B (Figure 6C), while Vegf-A was not expressed at levels sufficient
499 for reliable qPCR detection in these cells (Ct > 30). We also tested Vegf-B expression in
500 our three knockout cell lines (Figure 2), and observed a statistically significant, 40-60%
501 down-regulation of Vegf-B compared to control cells (Figure 6D). Upon ectopic
502 expression of *MaTAR20* in the KO cells, Vegf-B levels were up-regulated (Supplementary
503 Figure S7A). Based on convergent results obtained from four independent experiments
504 (ASO KD *in vitro*, *in vivo*, CRISPR/Cas9 promoter deletions and rescue assays), we
505 conclude that down-regulation of *MaTAR20* correlates with reduced VEGF expression
506 levels and may be associated with reduced tumor angiogenesis.

507 ***MaTAR20* loss leads to alterations in cancer signaling and adhesion pathways**

508 To identify how *MaTAR20* impacts Vegf signaling, we further investigated the
509 molecular mechanism by which the lncRNA acts. First, we performed differential RNA-
510 seq, comparing *MaTAR20* KO to control cells. A total of 223 genes were differentially
511 expressed ($p < 0.05$), with 129 genes down- and 94 genes up-regulated in the KO cells
512 (Figure 7A, Supplementary Figure S7B, Supplementary Table S2). Interestingly, one of
513 the most up-regulated genes was *Vascular endothelial growth inhibitor* (*Vegi*), also known
514 as *Tumor necrosis factor (TNF)-like cytokine 1A (TL1A)/TNF superfamily member 15*
515 (*Tnfsf15*). In agreement with our co-expression analysis (Figure 6A), we observed an
516 overall dysregulation of the VEGF signaling pathway and of hypoxia-inducible factor 1
517 (HIF-1) signaling, another pathway essential for angiogenesis (43) (Supplementary Table
518 S3). In addition, pathways involved in cancer signaling such as the MAPK, PI3K-Akt and

519 TNF axes were altered, as were several cell adhesion pathways, including "Focal
520 adhesion" and "Tight junctions" (Supplementary Table S3). Several of these pathways
521 were previously identified in our co-expression analysis as well (Figure 6A). Differential
522 expression of important cell signaling genes likely contributes to the altered phenotypes
523 we observed upon *MaTAR20* loss, such as reduced organoid branching and tumor cell
524 growth. Changes in cell adhesion pathways may explain the enhanced adhesion
525 phenotype observed in *MaTAR20* KO cells (Figure 2E), along with reduced migration and
526 metastatic burden upon KD of the lncRNA.

527 ***MaTAR20* regulates gene expression by direct binding to *Tnfsf15***

528 RNA-seq identifies all differentially expressed genes upon *MaTAR20* loss, both
529 effects due to direct binding and regulation of the gene by *MaTAR20*, as well as any
530 secondary or tertiary downstream effects. To hone in on direct targets of *MaTAR20*, we
531 performed Chromatin Isolation by RNA Purification (ChIRP, (44)) using two separate
532 pools of nine tiling oligonucleotides each. Both pools were able to enrich *MaTAR20*, with
533 pool 2 showing overall better pull-down performance (Figure 7B). The difference in
534 enrichment could be due to one or several oligonucleotides in pool 1 being obstructed
535 from binding to *MaTAR20*, caused by secondary structures or competition with putative
536 protein interaction partners. A negative control pull-down reaction for the mRNA
537 *cyclophilin B* (*CycloB*) was performed as well to control for unspecific binding of nucleic
538 acids to biotinylated oligonucleotides and/or streptavidin beads (Figure 7B).

539 We performed three independent replicates of ChIRP-seq with both probe pools
540 and *CycloB* negative control probes, and compared genes bound to *MaTAR20* in both
541 pools. The highest genomic peak score in both pools was as expected to the *MaTAR20*

542 locus itself, a similar observation was made in regard to *MaTAR25* lncRNA (13). Both
543 pool 1 and pool 2 were enriched for genes involved in cancer signaling and adhesion
544 pathways that were also identified in our RNA-seq analysis, such as PI3K-Akt and MAPK
545 signaling, "Focal adhesion" and "ECM-receptor interactions" (Supplementary Table S4).
546 The more efficient pool 2 pull-down was also enriched for VEGF and HIF-1 signaling
547 pathways (Supplementary Table S4). On an individual gene level, we assigned the
548 identified peaks to the nearest gene and were able to identify 574 genes bound by
549 *MaTAR20* in pool1 and 2,514 genes in pool 2 (excluding *MaTAR20* itself, as well as all
550 genes that were also found to bind to the negative control *CycloB* probe set)
551 (Supplementary Table S5), with an overlap of 182 target genes bound by *MaTAR20* in
552 both probe pools (Figure 7C, Supplementary Table S5).

553 Comparing RNA-seq and ChIRP-seq results, two genes were identified to be direct
554 binding partners of *MaTAR20* and also differentially expressed in *MaTAR20* KO cells
555 (Figure 7D): *Tnfsf15* and *Rab27b*. While *Tnfsf15* was significantly up-regulated upon
556 *MaTAR20* loss, *Rab27b* was repressed (Figure 7E). Up-regulation of *Tnfsf15* was
557 confirmed at the protein level in immunohistochemistry assays on tumor sections from
558 *MaTAR20* ASO treated animals (Supplementary Figure S6F). To further establish a direct
559 relationship between *MaTAR20* and *Tnfsf15* expression levels, we performed rescue
560 assays over-expressing ectopic *MaTAR20* in KO cells and observed decreased
561 expression of *Tnfsf15* as compared to the *MaTAR20* KO cells treated with just the
562 bavkbone plasmid (Supplementary Figure S7C).

563 We performed ChIRP-qPCR at the *Tnfsf15* gene locus to validate direct binding of
564 the lncRNA (Figure 6F). Our *MaTAR20* ChIRP-seq data identified two putative lncRNA

binding regions, one about 5 kb downstream and the second about 15 kb downstream of the *Tnfsf15* gene (Supplementary Figure S7D). We designed two primer pairs for each region (p1 and p2 for -15 kb, p3 and p4 for -5 kb), and a primer pair for a negative control region in between the two putative binding sites, at about -10 kb. Cyclo B probes served as a negative control for all tested regions, representing background noise. Our results indicate that both *MaTAR20* probe pools were able to specifically detect the lncRNA at the -5 kb site, while only the more efficient pool2 could also enrich for MaTAR20 at the -15 kb region. This may indicate higher levels of MaTAR20 binding to the *Tnfsf15* -5 kb site, which likely represents a *Tnfsf15* enhancer element. Overall, our results confirm that *MaTAR20* can regulate gene expression by directly binding to target genes such as *Tnfsf15*.

Based on our findings, we conclude that *MaTAR20* reduces or inhibits the expression of *Tnfsf15* by directly binding to its genomic locus. Tnfsf15 is a cytokine that has been described to inhibit VEGF expression (45) and, more generally, VEGF driven angiogenesis (46). Therefore, we hypothesize that loss of *MaTAR20* leads to reduced tumor angiogenesis (Figure 8). The proposed molecular mechanism agrees with the observed phenotype: delayed tumor onset, smaller tumors and increased necrosis, combined with lower metastatic burden in the lungs.

## Discussion

Here, we investigated *MaTAR20*, a lncRNA expressed at high levels in mammary tumors. Loss of *MaTAR20* by either ASO-mediated knockdown or CRISPR/Cas9 genome editing in mammary tumor cells leads to reduced proliferation, invasion and organoid

588 branching *in vitro*. In mouse models of BC, treatment with ASOs targeting *MaTAR20*
589 causes delayed tumor onset, reduced tumor growth and overall reduced metastatic
590 burden to the lungs. We were able to confirm the observed phenotype using different
591 ASO sequences, different ASO chemistries (MOE and cET), and in different mouse
592 background strains (FVB and C57/Bl6). Furthermore, our studies of human *MaTAR20* in
593 two loss-of-function and one gain-of-function models further corroborate that this lncRNA
594 is a driver of BC cell growth and migration and may represent a promising new therapeutic
595 target. We propose that ASOs targeting *MaTAR20* could be a viable new adjunct therapy,
596 as we obtained highly efficient lncRNA knockdown in tumors upon subcutaneous delivery.
597 We did not observe any adverse reactions in other mouse tissues or the animal overall,
598 potentially because *MaTAR20* is expressed at highest levels in the tumor, restricting the
599 effect of *MaTAR20* KD mostly to tumor tissue. Additional detailed studies of the human
600 orthologue *hMaTAR20* (7) will be essential to investigate the potential of the lncRNA as
601 a new therapeutic target in breast cancer. We observed cystic, differentiated metastases
602 in *MaTAR20* ASO-mediated mice, suggesting the treatment may have potential to impact
603 already existing metastases in the lungs. Future investigation of the impact of *MaTAR20*
604 on already existing metastatic nodules will be of particular value, as patients with
605 advanced disease would benefit from a therapeutic approach that is able to attack and/or
606 prevent the formation of metastases.

607 Our molecular data indicates that the nuclear-retained lncRNA *MaTAR20* drives
608 tumor growth and metastasis by impacting the expression of important cancer signaling
609 pathways and cell adhesion molecules. These findings are reflected in the observed
610 reduction of cell proliferation, migratory potential and formation of cell protrusions in 2D

611 and 3D cell culture systems. One particular pathway that stood out across all our analyses
612 is VEGF signaling and angiogenesis, seemingly centering on Vegf-B in our system.
613 VEGF-B produced by cancer cells has been described to lead to leaky vascular networks,
614 which in turn enables the tumor to invade its surrounding tissue with high efficiency (47).
615 In addition, high VEGF-B levels were associated with poor prognosis (47). Inhibition of
616 tumor-specific VEGF-B has been suggested as an interesting approach to inhibit cancer
617 progression and metastasis, with VEGF-B knockdown leading to reduced pulmonary
618 metastasis in a mouse model of melanoma (47). As *MaTAR20* also leads to reduced lung
619 metastatic nodules, we hypothesize that it may do so by regulating Vegf-B expression. In
620 addition, non-angiogenic functions of VEGF-B have been described previously in the
621 context of invasive BC, which could also play a role here (48).

622 Our ChIRP assays indicate that *MaTAR20* does not directly bind to the *Vegf-B*
623 gene, but to a number of other angiogenesis-related genes such as *angiopoietin 2*, among
624 many others. Of the 182 genes identified by ChIRP-seq analysis, two also show altered
625 expression in *MaTAR20* KO cells: *Tnfsf15* and *Rab27b*. Tnfsf15 is a cytokine usually
626 expressed in established vasculature but down-regulated in cancer lesions to allow for
627 neovascularization (46,49,50). Vegf and Tnfsf15 serve opposing functions, with carefully
628 balanced expression modulation of both factors playing key roles in vascular and immune
629 homeostasis. We suggest that *MaTAR20* regulates the balance of these proteins by
630 directly binding to the *Tnfsf15* locus and repressing the gene during tumor progression
631 (Figure 8). Reduced Tnfsf15 levels allow the tumor to recruit blood vessels, which is
632 essential for sustained tumor growth and enables intravasation of cancer cells into the
633 circulation, leading to metastasis (Figure 8A). In the absence of *MaTAR20*, we

634 hypothesize that Tnfsf15 expression will be re-activated and neovascularization of the
635 tumor is inhibited, which would agree with our observed reduction in Vegf-A, Vegf-B and
636 CD31+ cells (Figure 8B). In BC, high levels of Tnfsf15 in clinical samples were associated
637 with disease-free survival and overall better prognosis (51). This further solidifies our
638 hypothesis that tumor-specific up-regulation of Tnfsf15 via ASO-mediated *MaTAR20*
639 knockdown could be a promising therapeutic approach. As the lncRNA is expressed in
640 high levels only in cancer lesions, we suggest that consequences of *MaTAR20* KD,
641 including reduced neovascularization, are restricted to tumor tissue as well, representing
642 an attractive new approach of tumor-specific inhibition of angiogenesis.

643 In addition to regulating angiogenesis, Tnfsf15 has also been described to be
644 involved in dendritic cell maturation and T-cell co-activation (50). Future studies are
645 required to conclude if loss of *MaTAR20* also impacts immune cells in a cancer context,
646 or if the observed phenotype is in fact driven by reduced vascularization. Further
647 investigation is also required into the second identified *MaTAR20* target gene, *Rab27b*.
648 The small secretory GTPase has been described to control vesicle exocytosis and to
649 deliver pro-invasive growth regulators into the tumor microenvironment (52), and has
650 recently been associated with VEGF signaling in cancer as well (53). Rab27b has been
651 reported to promote proliferation and invasiveness of ER+ BC cells *in vitro* and *in vivo*,
652 and has been associated with lymph node metastasis and differentiation grade in ER+
653 human tumors (54). We observed that loss of *MaTAR20* leads to reduced Rab27b
654 expression, which may further contribute to the decrease in proliferative and migratory
655 potential we observed here. Future studies will elucidate the detailed regulatory
656 mechanism of Rab27b by *MaTAR20*.

**Acknowledgements**

We thank members of the Spector and Diermeier labs for critical discussions and advice throughout the course of this study. We thank Dr. Mikala Egeblad (CSHL) for providing MMTV-PyMT mice and Dr. Fred R. Miller (Wayne State University) for providing 4T1 cells. We acknowledge the CSHL Cancer Center Shared Resources (Microscopy, Flow Cytometry, Animal, Histology, and Next-Gen Sequencing) for services and technical expertise (NCI 2P3OCA45508). We thank David Jackson (CSHL) and Zachary Lippman (CSHL) for facilitating access to the SEM instruments. MCF10A and T47D cells used in this study were a generous gift of the Dunbier lab (Department of Biochemistry, University of Otago). We would also like to thank Robert Porteous and the Histology facility at the University of Otago and Bronwyn Carlisle (Department of Biochemistry) for her assistance with the *MaTAR20* model illustration (Figure 8).

673 **References**


674 1. Siegel RL, Miller KD, Fuchs HE, Jemal A. Cancer Statistics, 2021. CA: A Cancer
675 Journal for Clinicians. American Cancer Society; 2021;71:7–33.

676 2. Gupta RA, Shah N, Wang KC, Kim J, Horlings HM, Wong DJ, et al. Long non-
677 coding RNA HOTAIR reprograms chromatin state to promote cancer metastasis.
678 Nature. 2010;464:1071–6.

679 3. Prensner JR, Iyer MK, Balbin OA, Dhanasekaran SM, Cao Q, Brenner JC, et al.
680 Transcriptome sequencing across a prostate cancer cohort identifies PCAT-1, an
681 unannotated lincRNA implicated in disease progression. Nat Biotechnol.
682 2011;29:742–9.

683 4. Tseng Y-Y, Moriarity BS, Gong W, Akiyama R, Tiwari A, Kawakami H, et al. PVT1
684 dependence in cancer with MYC copy-number increase. Nature. 2014.

685 5. Xing Z, Lin A, Li C, Liang K, Wang S, Liu Y, et al. lncRNA directs cooperative
686 epigenetic regulation downstream of chemokine signals. 2014;159:1110–25.

687 6. Arun G, Diermeier S, Akerman M, Chang K-C, Wilkinson JE, Hearn S, et al.
688 Differentiation of mammary tumors and reduction in metastasis upon Malat1
689 lncRNA loss. Genes & Development. 2016;30:34–51.

690 7. Diermeier SD, Chang K-C, Freier SM, Song J, Demerdash El O, Krasnitz A, et al.
691 Mammary Tumor-Associated RNAs Impact Tumor Cell Proliferation, Invasion, and
692 Migration. Cell Reports. 2016;17:261–74.

693 8. Chakravarty D, Sboner A, Nair SS, Giannopoulou E, Li R, Hennig S, et al. The
694 oestrogen receptor alpha-regulated lncRNA NEAT1 is a critical modulator of
695 prostate cancer. Nature Communications. Nature Publishing Group;
696 2014;5:5383–16.

697 9. Sang L-J, Ju H-Q, Liu G-P, Tian T, Ma G-L, Lu Y-X, et al. LncRNA CamK-A
698 Regulates Ca2+-Signaling-Mediated Tumor Microenvironment Remodeling.
699 Molecular Cell. Elsevier Inc; 2018;72:71–7.

700 10. Hu Q, Ye Y, Chan L-C, Li Y, Liang K, Lin A, et al. Oncogenic lncRNA
701 downregulates cancer cell antigen presentation and intrinsic tumor suppression.
702 Nature Immunology. Springer US; 2019;:1–24.

703 11. Luo H, Zhu G, Xu J, Lai Q, Yan B, Guo Y, et al. HOTTIP lncRNA Promotes
704 Hematopoietic Stem Cell Self-Renewal Leading to AML-like Disease in Mice.
705 Cancer Cell. Elsevier Inc; 2019;:1–24.

706 12. Silva-Fisher JM, Dang HX, White NM, Strand MS, Krasnick BA, Rozycki EB, et al.
707 Long non-coding RNA RAMS11 promotes metastatic colorectal cancer
708 progression. Nature Communications. 2020;11:2156.

709 13. Chang K-C, Diermeier SD, Yu AT, Brine LD, Russo S, Bhatia S, et al. MaTAR25
710 lncRNA regulates the Tensin1 gene to impact breast cancer progression. Nature
711 Communications. Springer US; 2020;:1–19.

712 14. Yan X, Hu Z, Feng Y, Hu X, Yuan J, Zhao SD, et al. Comprehensive Genomic
713 Characterization of Long Non-coding RNAs across Human Cancers. Cancer Cell.
714 Elsevier Inc; 2015;28:529–40.

715 15. Ransohoff JD, Wei Y, Khavari PA. The functions and unique features of long
716 intergenic non-coding RNA. Nature Reviews Molecular Cell Biology. Nature
717 Publishing Group; 2018;19:143–57.

718 16. Huarte M. The emerging role of lncRNAs in cancer. Nature Medicine.
719 2015;21:1253–61.

720 17. Arun G, Diermeier SD, Spector DL. Therapeutic Targeting of Long Non-Coding
721 RNAs in Cancer. Trends Mol Med. 2018;24:257–77.

722 18. Gutschner T, Hammerle M, Eissmann M, Hsu J, Kim Y, Hung G, et al. The
723 Noncoding RNA MALAT1 Is a Critical Regulator of the Metastasis Phenotype of
724 Lung Cancer Cells. Cancer Research. 2013;73:1180–9.

725 19. Ewald AJ. Isolation of mouse mammary organoids for long-term time-lapse
726 imaging. Cold Spring Harb Protoc. 2013;2013:130–3.

727 20. Park J, Wysocki RW, Amoozgar Z, Maiorino L, Fein MR, Jorns J, et al. Cancer
728 cells induce metastasis-supporting neutrophil extracellular DNA traps. Sci Transl
729 Med. 2016;8:361ra138.

730 21. Nowak DG, Katsenelson KC, Watrud KE, Chen M, Mathew G, D'Andrea VD, et al.
731 The PHLPP2 phosphatase is a druggable driver of prostate cancer progression.
732 The Journal of Cell Biology. 2019;218:1943–57.

733 22. Minn AJ, Gupta GP, Siegel PM, Bos PD, Shu W, Giri DD, et al. Genes that
734 mediate breast cancer metastasis to lung. Nat Cell Biol. 2005;436:518–24.

735 23. Tanenbaum ME, Gilbert LA, Qi LS, Weissman JS, Vale RD. A Protein-Tagging
736 System for Signal Amplification in Gene Expression and Fluorescence Imaging.
737 Cell. Elsevier Inc; 2014;159:635–46.

738 24. Liang C-C, Park AY, Guan J-L. In vitro scratch assay: a convenient and
739 inexpensive method for analysis of cell migration in vitro. Nat Protoc. 2007;2:329–
740 33.

741 25. Guy CT, Cardiff RD, Muller WJ. Induction of mammary tumors by expression of
742 polyomavirus middle T oncogene: a transgenic mouse model for metastatic
743 disease. Molecular and Cellular Biology. 1992;12:954–61.

26. Bankhead P, Loughrey MB, ndez JXAFX, Dombrowski Y, McArt DG, Dunne PD, et al. QuPath: Open source software for digital pathology image analysis. Sci Rep. Springer US; 2017;:1–7.

27. Dobin A, Davis CA, Schlesinger F, Drenkow J, Zaleski C, Jha S, et al. STAR: ultrafast universal RNA-seq aligner. Bioinformatics. 2012;29:15–21.

28. Anders S, Pyl PT, Huber W. HTSeq--a Python framework to work with high-throughput sequencing data. Bioinformatics. 2015;31:166–9.

29. Love MI, Huber W, Anders S. Moderated estimation of fold change and dispersion for RNA-seq data with DESeq2. Genome Biol. 2014;15:550.

30. Luo W, Friedman MS, Shedden K, Hankenson KD, Woolf PJ. GAGE: generally applicable gene set enrichment for pathway analysis. BMC Bioinformatics. 2009;10:161.

31. Luo W, Brouwer C. Pathview: an R/Bioconductor package for pathway-based data integration and visualization. Bioinformatics. 2013;29:1830–1.

32. Langmead B, Salzberg SL. Fast gapped-read alignment with Bowtie 2. Nature Methods. 2012;9:357–9.

33. Heinz S, Benner C, Spann N, Bertolino E, Lin YC, Laslo P, et al. Simple Combinations of Lineage-Determining Transcription Factors Prime cis-Regulatory Elements Required for Macrophage and B Cell Identities. Molecular Cell. Elsevier Inc; 2010;38:576–89.

34. Diermeier SD, Spector DL. Antisense Oligonucleotide-mediated Knockdown in Mammary Tumor Organoids. BIO-PROTOCOL. 2017;7.

35. Tuveson D, Clevers H. Cancer modeling meets human organoid technology. Science. American Association for the Advancement of Science; 2019;364:952–5.

36. Shamir ER, Ewald AJ. Three-dimensional organotypic culture: experimental models of mammalian biology and disease. Nature Reviews Molecular Cell Biology. Nature Publishing Group; 2014;15:647–64.

37. Aslakson CJ, Miller FR. Selective events in the metastatic process defined by analysis of the sequential dissemination of subpopulations of a mouse mammary tumor. Cancer Research. 1992;52:1399–405.

38. Pallan PS, Allerson CR, Berdeja A, Seth PP, Swayze EE, Prakash TP, et al. Structure and nuclease resistance of 2′,4′-constrained 2′-O-methoxyethyl (cMOE) and 2′-O-ethyl (cEt) modified DNAs. Chem Commun. The Royal Society of Chemistry; 2012;48:8195–10.

39. Shen X, Corey DR. Chemistry, mechanism and clinical status of antisense oligonucleotides and duplex RNAs. Nucleic Acids Res. 2018;46:1584–600.

40. Jiang Q, Ma R, Wang J, Wu X, Jin S, Peng J, et al. LncRNA2Function: a comprehensive resource for functional investigation of human lncRNAs based on RNA-seq data. BMC Genomics. 2015;16 Suppl 3:S2.

41. Guttman M, Amit I, Garber M, French C, Lin MF, Feldser D, et al. Chromatin signature reveals over a thousand highly conserved large non-coding RNAs in mammals. Nature [Internet]. Nature Publishing Group; 2009;457:223–7. Available from: http://www.nature.com/doifinder/10.1038/nature07672

42. Wilhelm SM, Adnane L, Newell P, Villanueva A, Llovet JM, Lynch M. Preclinical overview of sorafenib, a multikinase inhibitor that targets both Raf and VEGF and PDGF receptor tyrosine kinase signaling. Mol Cancer Ther. 2008;7:3129–40.

43. Semenza GL. Targeting HIF-1 for cancer therapy. Nat Rev Cancer. Nature Publishing Group; 2003;3:721–32.

44. Chu C, Qu K, Zhong FL, Artandi SE, Chang HY. Genomic Maps of Long Noncoding RNA Occupancy Reveal Principles of RNA-Chromatin Interactions. Molecular Cell. Elsevier Inc; 2011;44:667–78.

45. Zhang K, Cai H-X, Gao S, Yang G-L, Deng H-T, Xu G-C, et al. TNFSF15 suppresses VEGF production in endothelial cells by stimulating miR-29b expression via activation of JNK-GATA3 signals. Oncotarget. Impact Journals; 2016;7:69436–49.

46. Yang G-L, Li L-Y. Counterbalance: modulation of VEGF/VEGFR activities by TNFSF15. Signal Transduction and Targeted Therapy. Springer US; 2018;:1–7.

47. Yang X, Zhang Y, Hosaka K, Andersson P, Wang J, Tholander F, et al. VEGF-B promotes cancer metastasis through a VEGF-A–independent mechanism and serves as a marker of poor prognosis for cancer patients. Proceedings of the National Academy of Sciences. 2015;112:E2900–9.

48. Gunningham SP, Currie MJ, Han C, Robinson BA, Scott PA, Harris AL, et al. VEGF-B expression in human primary breast cancers is associated with lymph node metastasis but not angiogenesis. J Pathol. John Wiley & Sons, Ltd; 2001;193:325–32.

49. Deng W, Gu X, Lu Y, Gu C, Zheng Y, Zhang Z, et al. Down-modulation of TNFSF15 in ovarian cancer by VEGF and MCP-1 is a pre-requisite for tumor neovascularization. Angiogenesis. Springer Netherlands; 2011;15:71–85.

50. Zhang Z, Li L-Y. TNFSF15 Modulates Neovascularization and Inflammation. Cancer Microenvironment. 2012;5:237–47.

814 51. Parr C, Gan CH, Watkins G, Jiang WG. Reduced vascular endothelial growth
815 inhibitor (VEGI) expression is associated with poor prognosis in breast cancer
816 patients. Angiogenesis. 2006;9:73–81.

817 52. Hendrix A, Maynard D, Pauwels P, Braems G, Denys H, Van den Broecke R, et
818 al. Effect of the Secretory Small GTPase Rab27B on Breast Cancer Growth,
819 Invasion, and Metastasis. J Natl Cancer Inst. 2010;102:866–80.

820 53. Tsuruda M, Yoshino H, Okamura S, Kuroshima K, Osako Y, Sakaguchi T, et al.
821 Oncogenic effects of RAB27B through exosome independent function in renal cell
822 carcinoma including sunitinib-resistant. Dahiya R, editor. PLoS ONE.
823 2020;15:e0232545–20.

824 54. Li Z, Fang R, Fang J, He S, Liu T. Functional implications of Rab27 GTPases in
825 Cancer. Cell Communication and Signaling; 2018;:1–8.

826

827 **Figure Legends**

828

829 **Figure 1: *MaTAR20* is a tumor-specific, nuclear-retained lncRNA**

830 **A:** Schematic overview of the *MaTAR20*/*Gm13387* locus (UCSC Browser, mm10)
831 GENCODE vM18 annotation in green.

832 **B:** Abundance (FPKM) of *MaTAR20* in ENCODE mouse tissue and HER2+ mammary
833 tumors.

834 **C:** Single molecule RNA FISH of MaTAR20 in primary MMTV-PyMT cells. Top panel:
835 merge, middle panel: MaTAR20 (red), bottom panel: DAPI (blue).

836 **D:** Cellular fractionation assay followed by qRT-PCR.

837 **E:** ASO-mediated knockdown of MaTAR20 in primary MMTV-PyMT organoids. Two
838 specific ASOs were tested for MaTAR20, and a scASO was used as negative control.
839 Bars denote the mean of at least two biological replicates +/- SD.

840 **F:** Quantification of organoid branching upon MaTAR20 knockdown. Bars denote the
841 mean of at least three biological replicates +/- SD.

842 **G:** Exemplarily images of organoids quantified in F.

843 **H:** Exemplarily SEM micrograph of organoids quantified in F.

844

845 **Figure 2: *MaTAR20* KO cells show reduced proliferation and cell adhesion**

846 Statistical significance was determined with a two-way ANOVA; * $p < 0.05$, ** $p < 0.01$.

847 **A:** Schematic overview of the knockout strategy. Guide RNAs (gRNAs) are indicated in
848 red, +/- indicate genomic position relative to the *MaTAR20* transcription start site.

849 **B**: qRT-PCR to determine relative *MaTAR20* expression in *MaTAR20* promoter deletion
850 cell lines. KO = promoter deletion of 748 bp (combination of gRNAs "+12" and "-736"),
851 Ren = negative control, integration of Cas9 and a gRNA targeting *Renilla* luciferase. Bars
852 denote the mean of at least six biological replicates +/- SEM.
853 **C**: Cell proliferation assay. Number of cells determined after 24, 48 and 72h. Data points
854 denote the mean of at least two biological replicates +/- SEM.
855 **D:** Cell cycle profiles of NST-DAPI stained cells, comparing Ren control cells to KO1 and
856 KO2.
857 **E:** Scanning electron micrograph of control (Ren) or CRISPR/Cas9-modified cells (KO).
858 Scale as indicated.
859
860 **Figure 3: Human *MaTAR20* (*hMaTAR20*) drives cell proliferation and migration**
861 Bars denote the mean of three biological replicates +/- SEM. * $p < 0.05$, ** $p < 0.01$, *** $p$
862 $< 0.001$.
863 **A:** Analysis of *hMaTAR20* expression in TCGA data, by subtype. LumA = luminal A, LumB
864 = luminal B, NL = normal-like breast cancer.
865 **B:** RNA-FISH of *hMaTAR20* on a tissue microarray (TMA), comparing expression in
866 breast cancer to corresponding normal breast tissue.
867 **C:** qRT-PCR to determine relative *hMaTAR20* expression in CRISPR/Cas9 edited T47D
868 cells. M888: control cell line with non-targeting sgRNA. KO C9 and KO V2: individual
869 single cell sorted colonies of T47D cells with a deletion in exon 1.
870 **D:** Cell proliferation assay comparing growth curves of the M888 negative control to the
871 two *hMaTAR20* KO clones.

872 **E:** Left: quantification of T47D spheroid branching (left). Right: exemplary images of the
873 negative control M888 (top) and the KO C2 clone (bottom). For each biological replicate,
874 n = 100 spheroids were analyzed (n = 300, total).
875 **F:** Quantification of T47D scratch assay.
876 **G:** qRT-PCR to determine relative *hMaTAR20* expression in MCF10A cells. The
877 endogenous *hMaTAR20* gene was up-regulated using CRISPRa using three specific
878 sgRNAs: -200, -270 and -390 (numbers denote the distance from the TSS). A non-
879 targeting sgRNA for *Renilla* luciferase served as a negative control (Ren).
880 **H:** Cell proliferation assay comparing growth curves of the Ren negative control to the
881 three *hMaTAR20* CRISPRa cell lines.
882 **I:** Quantification of MCF10A scratch assay.
883
884 **Figure 4: cET ASO-mediated knockdown of *MaTAR20* in 4T1 cells lead to reduced**
885 **cell proliferation and invasion**
886 Bars denote the mean of three biological replicates +/- SEM. Statistical significance was
887 determined with a two-tailed Student's t-test; * $p < 0.05$, ** $p < 0.01$, *** $p < 0.001$.
888 **A:** qRT-PCR to determine relative *MaTAR20* expression. 24 h post treatments with cET
889 ASOs (concentrations as indicated).
890 **B:** qRT-PCR to determine relative *MaTAR20* expression. 72 h post treatments with 0.5
891 µM cET ASOs.
892 **C:** Proliferation assay. Cells were counted 24 h and 72 h post treatment with 0.5 µM cET
893 ASOs.
894 **D:** Invasion assay. Fluorescence units 24 h post treatment with 0.5 µM cET ASOs.

895

896 **Figure 5: cET ASO-mediated knockdown of *MaTAR20 in vivo* lead to reduced tumor**

897 **growth and metastatic burden**

898 Statistical significance was determined with a two-tailed Student's t-test; * $p < 0.05$, ** $p$

899 $< 0.01$, *** $p < 0.001$.

900 **A:** MMTV-PyMT (C57/Bl6) mice were treated for 8 weeks with cET ASOs (100

901 mg/kg/week), either scASO (cET) or *MaTAR20* cET1. Bars / lines denote the mean of

902 biological replicates +/- SEM. N= 33 tumors from 7 mice for scASO (cET); n = 26 tumors

903 from 8 mice for *MaTAR20* cET1.

904 **B:** qRT-PCR to determine relative *MaTAR20* expression in tumors.

905 **C:** Average number of tumors per mouse in each treatment group.

906 **D:** Average tumor burden in $mm^3$ per week in each treatment group.

907 **E:** Hematoxylin and Eosin staining of tumor sections. Top left: scASO (cET) treated tumor

908 (whole tumor). Top right: scASO (cET) treated tumor, 10x. Bottom left: *MaTAR20* cET1

909 treated tumor (whole tumor). Bottom right: *MaTAR20* cET1 treated tumor, 10x.

910 **F:** Tumor growth curves of MDA-MB-231-LM2 cells were xenografted into nude mice.

911 Ren: a non-targeting negative control (n=10); -277: *hMaTAR20* CRISPRi cell line (n=9).

912 Data points denote the mean of biological replicates +/- SEM.

913 **G:** Quantification of tumor necrosis, based on H&E staining. Bars denote the mean of

914 three biological replicates +/- SEM.

915

916 **Figure 6: *MaTAR20* impacts VEGF expression**

917 Statistical significance was determined with a two-tailed Student's t-test; * $p < 0.05$, ** $p$
918 $< 0.01$.
919 **A:** Co-expression analysis to identify *MaTAR20* associated pathways. The 15 most
920 significant pathways are shown.
921 **B:** qRT-PCR to determine the relative Vegf-A and Vegf-B expression in tumors. MMTV-
922 PyMT mice were treated for 8 weeks with cET ASOs (100 mg/kg/week), either scASO
923 (cET) or *MaTAR20* cET1.
924 **C:** qRT-PCR to determine the relative Vegf-B expression in 4T1 cells. 72 h post
925 treatments with 0.5 µM cET ASOs. Bars denote the mean of three biological replicates
926 +/- SEM.
927 **D:** qRT-PCR to determine the relative Vegf-B expression in *MaTAR20* KO cells. Bars
928 denote the mean of two biological replicates +/- SEM.
929
930 **Figure 7: RNA-seq and ChIRP-seq identify *Tnfsf15* as a direct *MaTAR20* target gene**
931 **A:** RNA-seq. Heatmap of significantly differentially expressed genes comparing
932 *MaTAR20* KO and Ren cells. N1-3 indicate three independent biological replicates.
933 **B:** ChIRP-seq. qRT-PCR to determine the efficiency of the ChIRP assay. Both *MaTAR20*
934 probe pools enrich *MaTAR20*, with Pool 2 being more efficient. "Cyclo B" indicates a
935 separate pull-down experiment with oligonucleotides specific for the *cyclophilin B* mRNA,
936 which was used as a specificity control. Percentage of MaTAR20 or CycloB pull-down in
937 relation to input is shown. Bars denote the average of at least 3 replicates +/- SD.
938 **C:** ChIRP-seq. Venn diagram illustrating the overlap of ChIRP-seq performed with Pool1
939 vs Pool2 probes. Genes also identified in the negative control (Cyclo B) pull-down were

940 removed from the target lists. 183 genes overlap between both ChIRP probe pools, with
941 Pool1 enriching more genes than Pool 2 overall. All ChIRP experiments were performed
942 in three independent replicates.
943 **D:** Venn diagram illustrating the overlap of the 182 target genes identified by ChIRP-seq
944 and the 223 differentially expressed genes according to RNA-seq. 2 genes are both direct
945 genomic binding partners of *MaTAR20* and are differentially expressed upon *MaTAR20*
946 loss.
947 **E:** RNA-seq. Expression of Tnfsf15 and Rab27b, comparing the mean log2 fold-change
948 in the two *MaTAR20* KO cell lines ("MaTAR20 KO") to the mean log2 fold-change of the
949 Ren negative control cell lines ("Control").
950 **F**: qRT-PCR to validate direct *MaTAR20* binding to the *Tnfsf15* locus. Four tiling primer
951 pairs were designed to two putative *MaTAR20* binding regions in proximity to the *Tnfsf15*
952 gene. A negative control region, located between p1/p2 and p3/p4, shows no *MaTAR20*
953 enrichment. CycloB probes control for unspecific binding at all tested sites. Bars denote
954 the mean of at least two biological replicates +/- SD.
955
956 **Figure 8: *MaTAR20* knockdown leads to smaller, necrotic tumors and reduced**
957 **metastasis**
958 **A:** During cancer progression, tumors secret pro-angiogenic factors to recruit blood
959 vessels. Increased vasculature allows for steady tumor growth while also increasing the
960 chances for metastatic spread.
961 **B:** In the absence of *MaTAR20*, tumor growth is slowed down, tumor necrosis increases,
962 and metastasis is reduced. We hypothesize that this could be due to the observed down-

963 regulation of *Vegf-B*, which may in part be caused by direct binding of *MaTAR20* to
964 *Tnfsf15*. Additional players such as protein binding partners may be of importance and
965 will be elucidated further in future studies.
966
967 **Figure S1:**
968 **A:** qRT-PCR to determine relative *MaTAR20* expression in MMTV-PyMT tumors of
969 different size. "Small" tumors: <200 $mm^3$, n=7; "medium" tumors: 300 - 1000 $mm^3$, n=4;
970 "large" tumors: >1500 $mm^3$, n=3.
971
972 **Figure S2:**
973 **A:** qRT-PCR to determine the relative *MaTAR20* expression in mouse mammary tumor
974 cell lines. Bars denote the mean of three biological replicates +/- SD.
975 **B:** qRT-PCR to determine the relative expression of individual MaTAR20 isoforms in
976 *MaTAR20* promoter deletion cell lines. KO = promoter deletion of 748 bp (combination of
977 gRNAs "+12" and "-736"), Ren = negative control, integration of Cas9 and a gRNA
978 targeting *Renilla* luciferase. Bars denote the mean of two biological replicates +/- SD.
979 **C:** Correlation of *MaTAR20* expression (all isoforms, based on six biological replicates,
980 Figure 2B) and Cas9 expression, as determined by qRT-PCR in three biological
981 replicates.
982
983 **Figure S3:**
984 **A:** Cell proliferation assay. Number of cells determined after 48 h. Statistical significance
985 was determined comparing KO cells transfected with a *MaTAR20* Tx1 (KO+MaTAR20)
986 to KO cells transfected with an empty backbone (KO+bb) and untransfected KO cells.

987 Control Ren cells are shown for reference. Error bars denote SD, and a two-tailed
988 Student's t-test was performed comparing KO+bb to KO+*MaTAR20*; * $p < 0.05$.
989 **B:** Cell proliferation assay comparing *MaTAR20* isoform 1 and isoform 2 after 24 and 48
990 h. Cell counts normalized to KO cells transfected with empty vector (bb). Bars denote the
991 mean of at least two biological replicates +/- SD. Statistical significance was determined
992 with a two-tailed Student's t-test comparing KO+bb to KO+*MaTAR20*; * $p < 0.05$, ** $p <$
993 $0.01$.
994
995 **Figure S4:**
996 **A:** RNA-FISH of *hMaTAR20* on a tissue microarray (TMA), comparing expression in
997 breast cancer of different grades to corresponding normal breast tissue. Statistical
998 significance was determined with a one-way ANOVA; *** $p < 0.001$.
999 **B:** qRT-PCR to determine relative *hMaTAR20* expression in a panel of breast cancer
1000 cells. Bars denote the mean of three biological replicates +/- SEM. Statistical significance
1001 was determined with a one-way ANOVA ;**** $p < 0.0001$.
1002 **C:** RNA-FISH of *hMaTAR20* in MDA-MB-231-LM2 (LM2).
1003 **D:** qRT-PCR to determine relative *hMaTAR20* expression in MDA-MB-231-LM2 (LM2)
1004 cells. Ren: control cell line with non-targeting sgRNA. -277; -390: CRISPRi *hMaTAR20*
1005 knockdown cell lines, numbers denote distance to the TSS. Bars denote the mean of at
1006 least three biological replicates +/- SEM. Statistical significance was determined with a
1007 two-tailed Student's t-test; * $p < 0.05$.

1008 **E:** Quantification of LM2 scratch assay. Bars denote the mean of at least three biological
1009 replicates +/- SEM. Statistical significance was determined with a two-tailed Student's t-
1010 test; * $p < 0.05$.
1011 **F:** Cell proliferation assay comparing growth curves of the Ren negative control to the two
1012 *hMaTAR20* KD cell lines. Data points denote the mean of at least three biological
1013 replicates +/- SEM.
1014 **G:** Quantification of LM2 spheroid branching. For each biological replicate, n = 100
1015 spheroids were analyzed (n = 300, total). Bars denote the mean of at least three biological
1016 replicates +/- SEM. Statistical significance was determined with a two-tailed Student's t-
1017 test; * $p < 0.05$.
1018
1019 **Figure S5:**
1020 **A:** Related to Figure 5, cET experiments: quantification of macro-metastatic nodules,
1021 displayed is the average number per lung.
1022 **B:** Related to Figure 5, cET experiments: Hematoxylin and Eosin staining of fixed lung
1023 sections.
1024 **C:** Related to Figure 5, cET experiments: quantification of metastases by area. Bars
1025 represent the mean +/- SEM.
1026 **D:** MMTV-PyMT (FVB) mice were treated for 6 weeks with MOE ASOs (150 mg/kg/week),
1027 either scASO or *MaTAR20* ASO1. Bars / lines denote the mean of biological replicates
1028 +/- SEM.
1029 **E:** Average tumor burden in $mm^3$ per week in each treatment group, tumor size 100-200
1030 $mm^3$, n=5 tumors.

1031 **F:** Quantification of macro-metastatic nodules, displayed is the average number per lung.
1032 Insets show exemplary images of lungs from scASO and ASO1 treated animals.
1033 **G:** Hematoxylin and Eosin staining of tumor sections. Left: scASO treated tumor. Right:
1034 *MaTAR20* ASO1 treated tumor.
1035
1036 **Figure S6:**
1037 Immunohistochemistry on tumors from animals treated with either scASO or *MaTAR20*
1038 ASO. "MOE" = animals in the 2'MOE ASO cohort, "cET" = animals in the cET ASO cohort.
1039 Lines within boxplots indicate the median. The y-axis indicates the percentage of each
1040 tumor section stained with the respective antibody given a defined detection threshold
1041 (0.2 for CD31, 0.5 for all other antibodies). Two technical replicates were measured for
1042 each tumor. The axis indicates which ASO chemistry was used (MOE or cET).
1043 **A:** Ki67 staining
1044 **B:** Cleaved caspase-3 staining
1045 **C:** Vegf-A staining
1046 **D:** Vegf-B staining
1047 **E:** CD31 staining
1048 **F:** Tnfsf15 staining
1049
1050 **Figure S7:**
1051 **A:** qRT-PCR to determine the relative *Vegf-B* expression in 4T1 *MaTAR20* KO cells. Cells
1052 were transfected either with *MaTAR20* Tx1 (KO+MaTAR20) or an empty backbone

1053 (KO+bb). Bars denote the mean of at least three biological replicates +/- SD. Statistical

1054 significance was determined with a two-tailed Student's t-test; * $p < 0.05$

1055 **A:** Top 10 up-and down-regulated genes in *MaTAR20* KO cells compared to Ren control

1056 cells.

1057 **B:** Like A, for *Tnfsf15*.

1058 **C:** UCSC Browser image illustrating *MaTAR20* binding to the *Tnfsf15* locus.

1059
1060

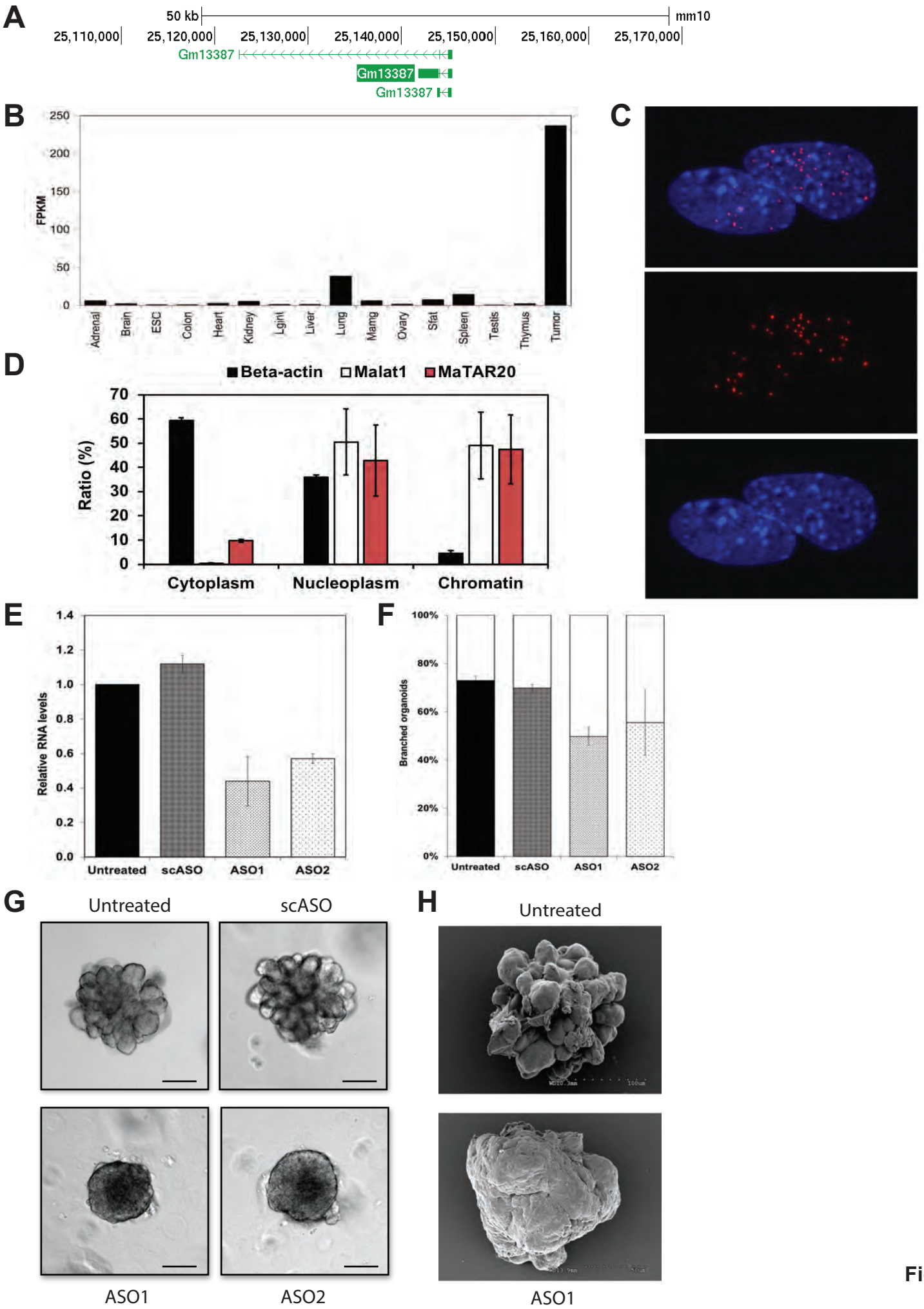
A
50 kb
mm10
25,110,000
25,120,000
25,130,000
25,140,000
25,150,000
25,160,000
25,170,000
Gm13387
Gm13387
Gm13387
B
FPKM
250
200
150
100
50
0
Adrenal
Brain
ESC
Colon
Heart
Kidney
Lgint
Liver
Lung
Mamg
Ovary
Sfat
Spleen
Testis
Thymus
Tumor
C
D
Beta-actin
Malat1
MaTAR20
Ratio (%)
70
60
50
40
30
20
10
0
Cytoplasm
Nucleoplasm
Chromatin
E
Relative RNA levels
1.4
1.2
1.0
0.8
0.6
0.4
0.2
0.0
Untreated
scASO
ASO1
ASO2
F
Branched organoids
100%
80%
60%
40%
20%
0%
Untreated
scASO
ASO1
ASO2
G
Untreated
scASO
ASO1
ASO2
H
Untreated
ASO1

Figure 1

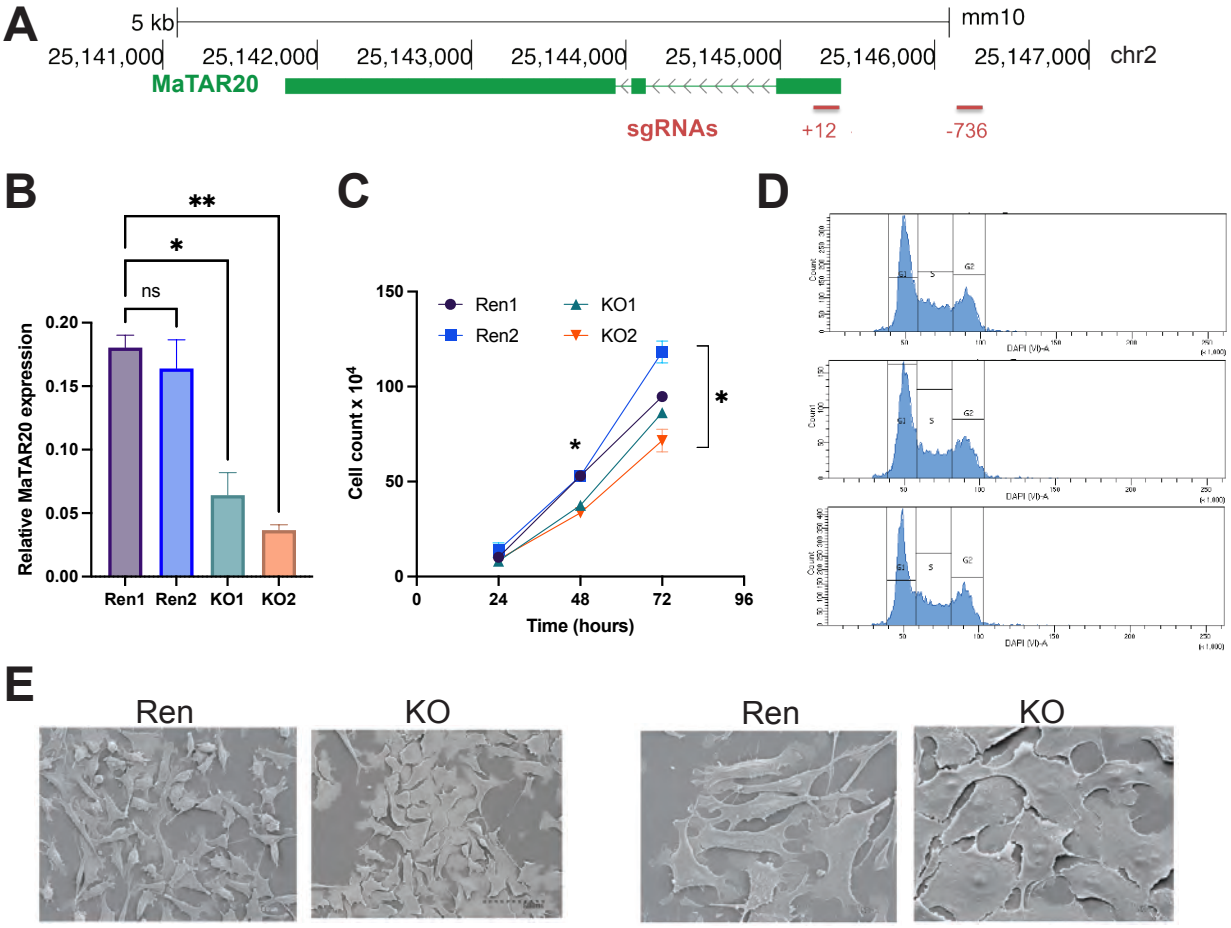
A
5 kb
mm10
25,141,000
25,142,000
25,143,000
25,144,000
25,145,000
25,146,000
25,147,000
chr2
MaTAR20
sgRNAs
+12
-736
B
**
*
ns
Relative MaTAR20 expression
0.20
0.15
0.10
0.05
0.00
Ren1
Ren2
KO1
KO2
C
Ren1
Ren2
KO1
KO2
Cell count x 10^4
150
100
50
0
0
24
48
72
96
Time (hours)
*
*
D
G1
S
G2
DAPI (VB-A
E
Ren
KO
Ren
KO

Figure 2

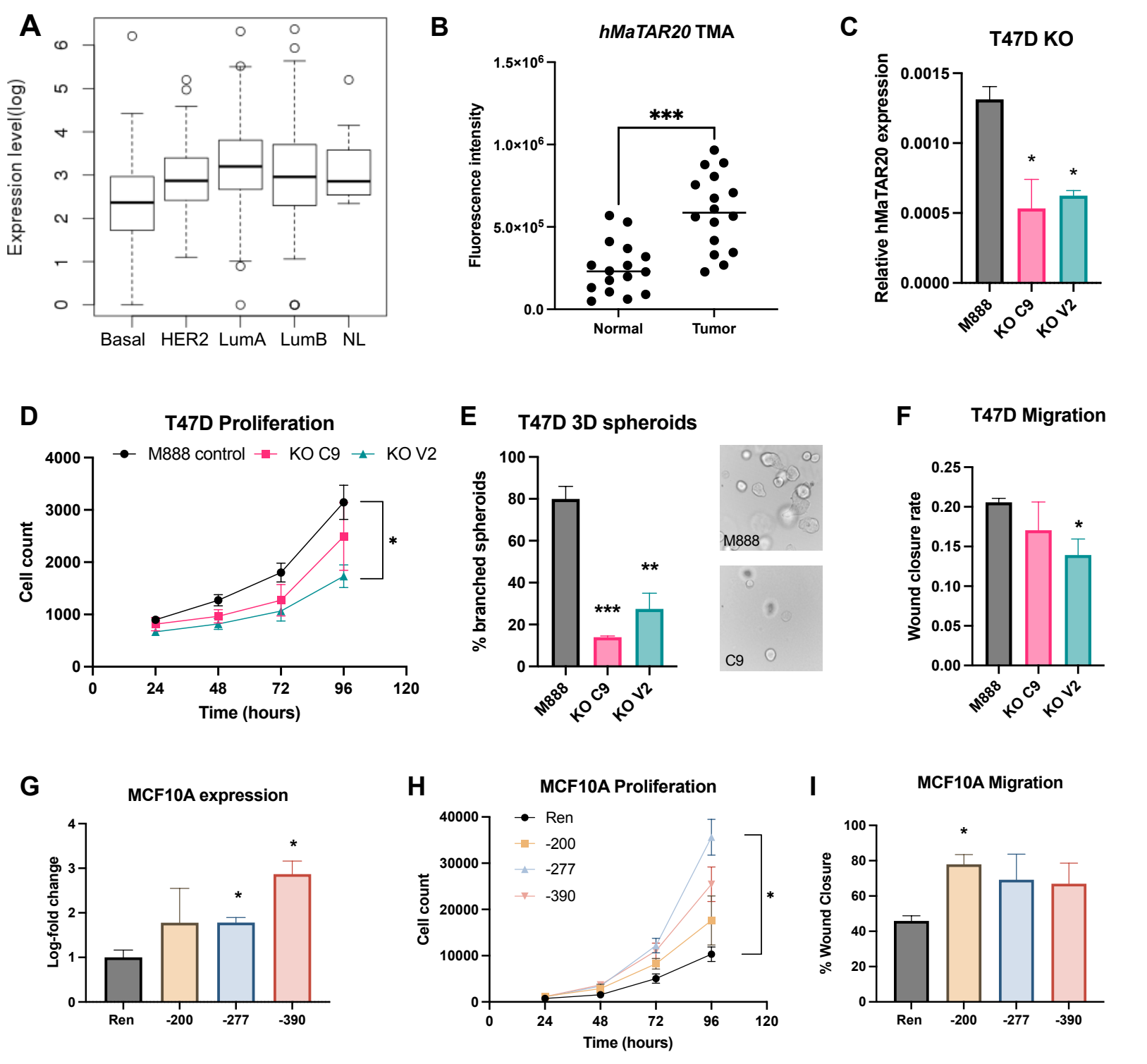
A
Expression level(log)
0
1
2
3
4
5
6
Basal
HER2
LumA
LumB
NL
B
hMaTAR20 TMA
Fluorescence intensity
1.5×10^6
1.0×10^6
5.0×10^5
0.0
***
Normal
Tumor
C
T47D KO
Relative hMaTAR20 expression
0.0015
0.0010
0.0005
0.0000
*
*
M888
KO C9
KO V2
D
T47D Proliferation
M888 control
KO C9
KO V2
Cell count
4000
3000
2000
1000
0
*
0
24
48
72
96
120
Time (hours)
E
T47D 3D spheroids
% branched spheroids
100
80
60
40
20
0
***
**
M888
KO C9
KO V2
M888
C9
F
T47D Migration
Wound closure rate
0.25
0.20
0.15
0.10
0.05
0.00
*
M888
KO C9
KO V2
G
MCF10A expression
Log-fold change
4
3
2
1
0
*
*
Ren
-200
-277
-390
H
MCF10A Proliferation
Ren
-200
-277
-390
Cell count
40000
30000
20000
10000
0
*
0
24
48
72
96
120
Time (hours)
I
MCF10A Migration
% Wound Closure
100
80
60
40
20
0
*
Ren
-200
-277
-390

Figure 3

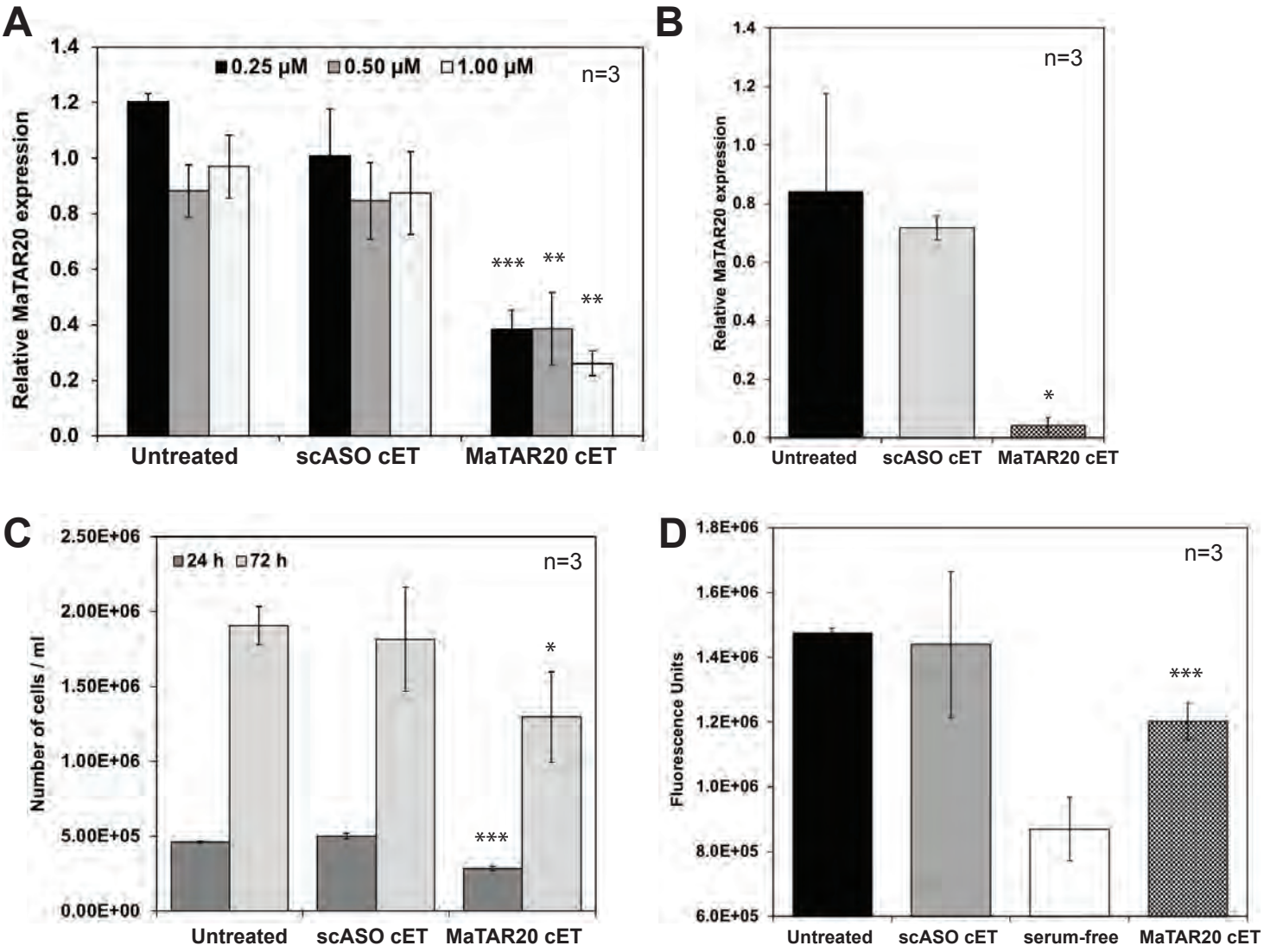
A
0.25 µM
0.50 µM
1.00 µM
n=3
Relative MaTAR20 expression
1.4
1.2
1.0
0.8
0.6
0.4
0.2
0.0
***
**
**
Untreated
scASO cET
MaTAR20 cET
B
n=3
Relative MaTAR20 expression
1.4
1.2
1.0
0.8
0.6
0.4
0.2
0.0
*
Untreated
scASO cET
MaTAR20 cET
C
24 h
72 h
n=3
Number of cells / ml
2.50E+06
2.00E+06
1.50E+06
1.00E+06
5.00E+05
0.00E+00
*
***
Untreated
scASO cET
MaTAR20 cET
D
n=3
Fluorescence Units
1.8E+06
1.6E+06
1.4E+06
1.2E+06
1.0E+06
8.0E+05
6.0E+05
***
Untreated
scASO cET
serum-free
MaTAR20 cET

Figure 4

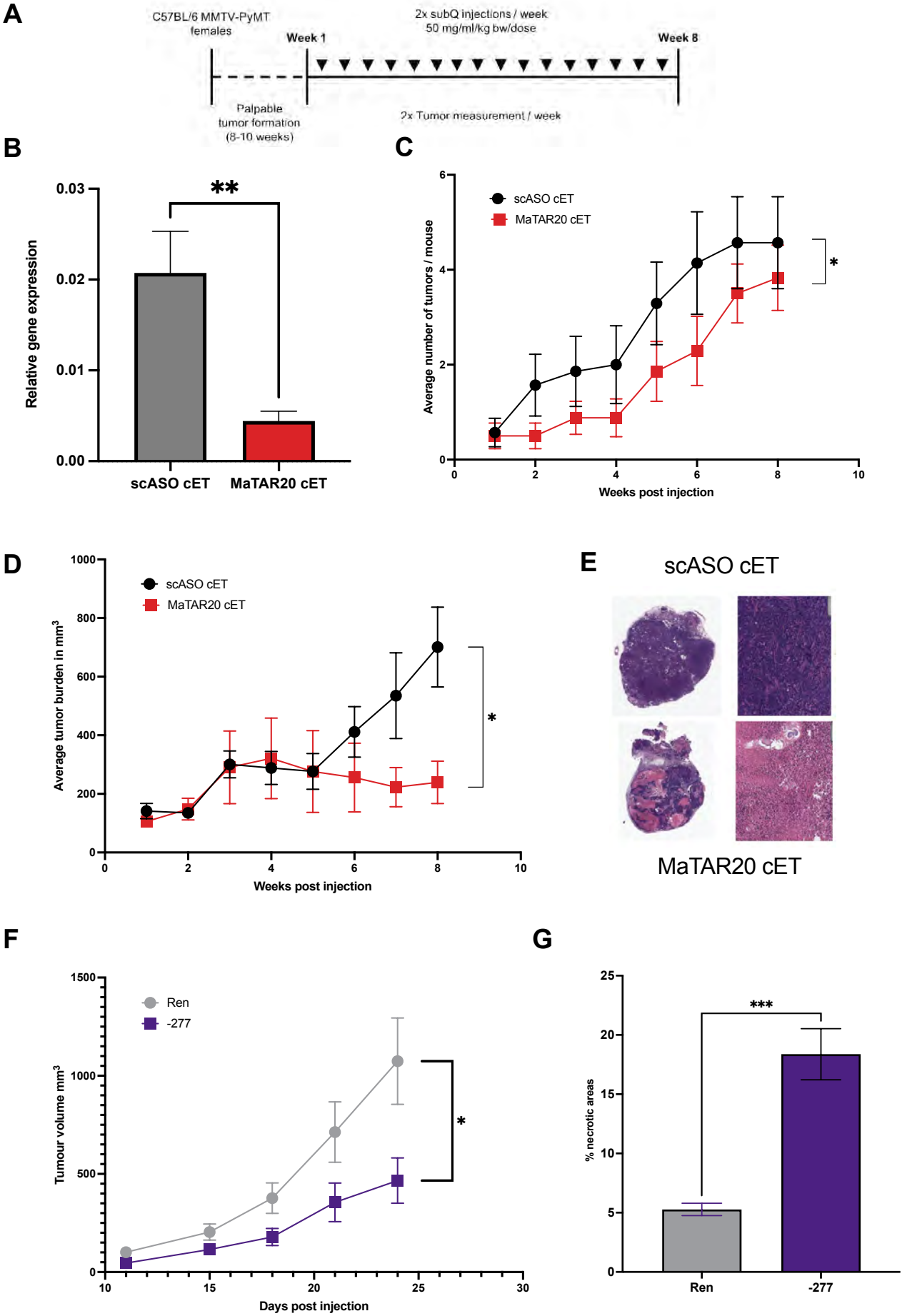
A
C57BL/6 MMTV-PyMT females
Week 1
2x subQ injections / week
50 mg/ml/kg bw/dose
Week 8
Palpable tumor formation (8-10 weeks)
2x Tumor measurement / week
B
Relative gene expression
0.03
0.02
0.01
0.00
**
scASO cET
MaTAR20 cET
C
Average number of tumors / mouse
scASO cET
MaTAR20 cET
*
Weeks post injection
D
Average tumor burden in mm3
scASO cET
MaTAR20 cET
*
Weeks post injection
E
scASO cET
MaTAR20 cET
F
Tumour volume mm3
Ren
-277
*
Days post injection
G
% necrotic areas
***
Ren
-277

Figure 5

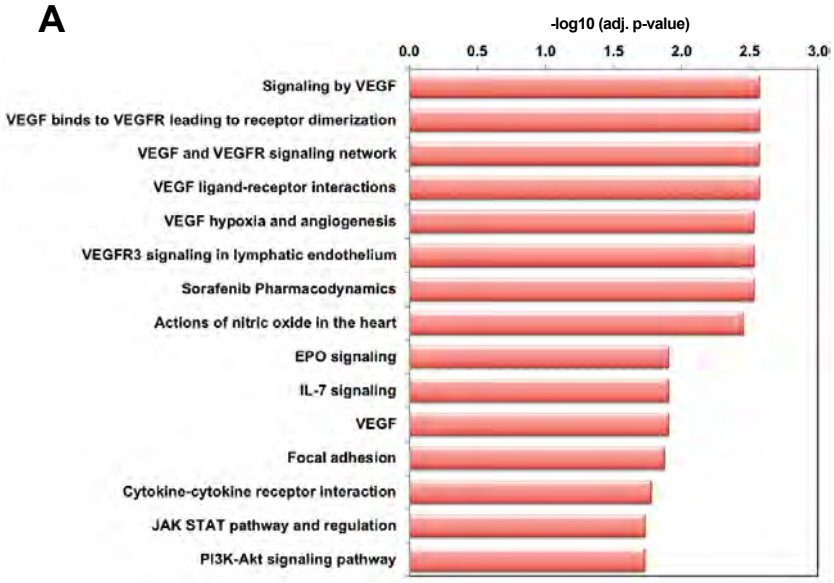
A
-log10 (adj. p-value)
0.0
0.5
1.0
1.5
2.0
2.5
3.0
Signaling by VEGF
VEGF binds to VEGFR leading to receptor dimerization
VEGF and VEGFR signaling network
VEGF ligand-receptor interactions
VEGF hypoxia and angiogenesis
VEGFR3 signaling in lymphatic endothelium
Sorafenib Pharmacodynamics
Actions of nitric oxide in the heart
EPO signaling
IL-7 signaling
VEGF
Focal adhesion
Cytokine-cytokine receptor interaction
JAK STAT pathway and regulation
PI3K-Akt signaling pathway

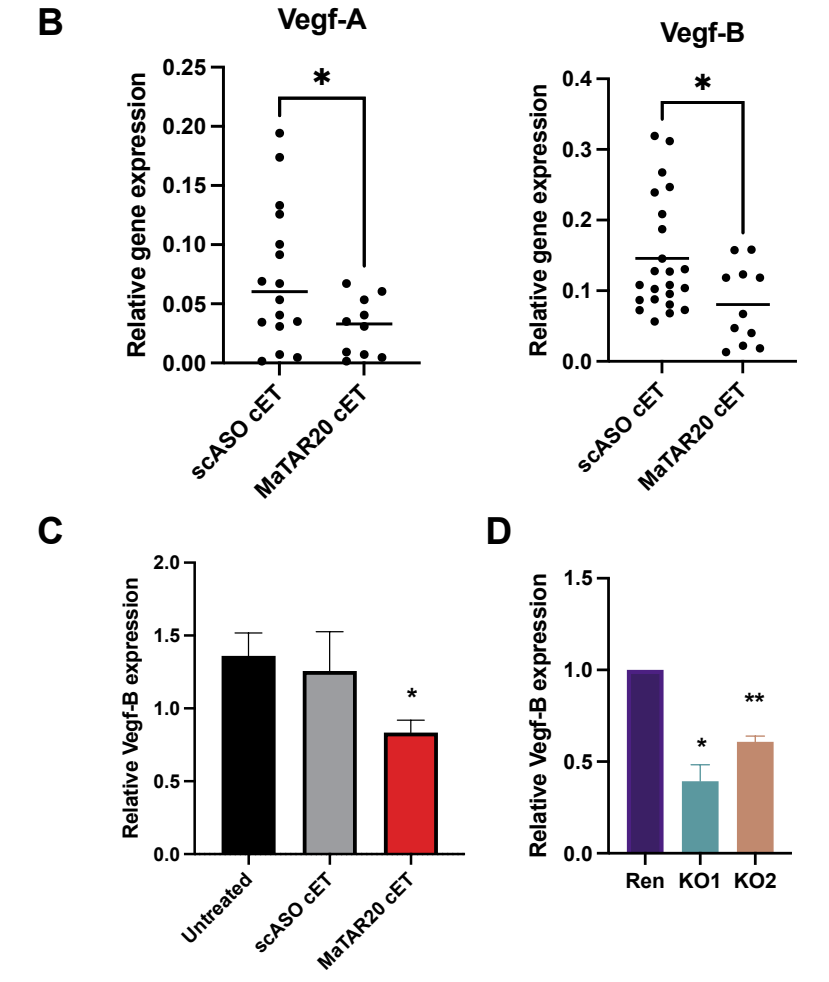
B
Vegf-A
Relative gene expression
0.25
0.20
0.15
0.10
0.05
0.00
*
scASO cET
MaTAR20 cET
Vegf-B
Relative gene expression
0.4
0.3
0.2
0.1
0.0
*
scASO cET
MaTAR20 cET
C
Relative Vegf-B expression
2.0
1.5
1.0
0.5
0.0
*
Untreated
scASO cET
MaTAR20 cET
D
Relative Vegf-B expression
1.5
1.0
0.5
0.0
*
**
Ren
KO1
KO2

Figure 6

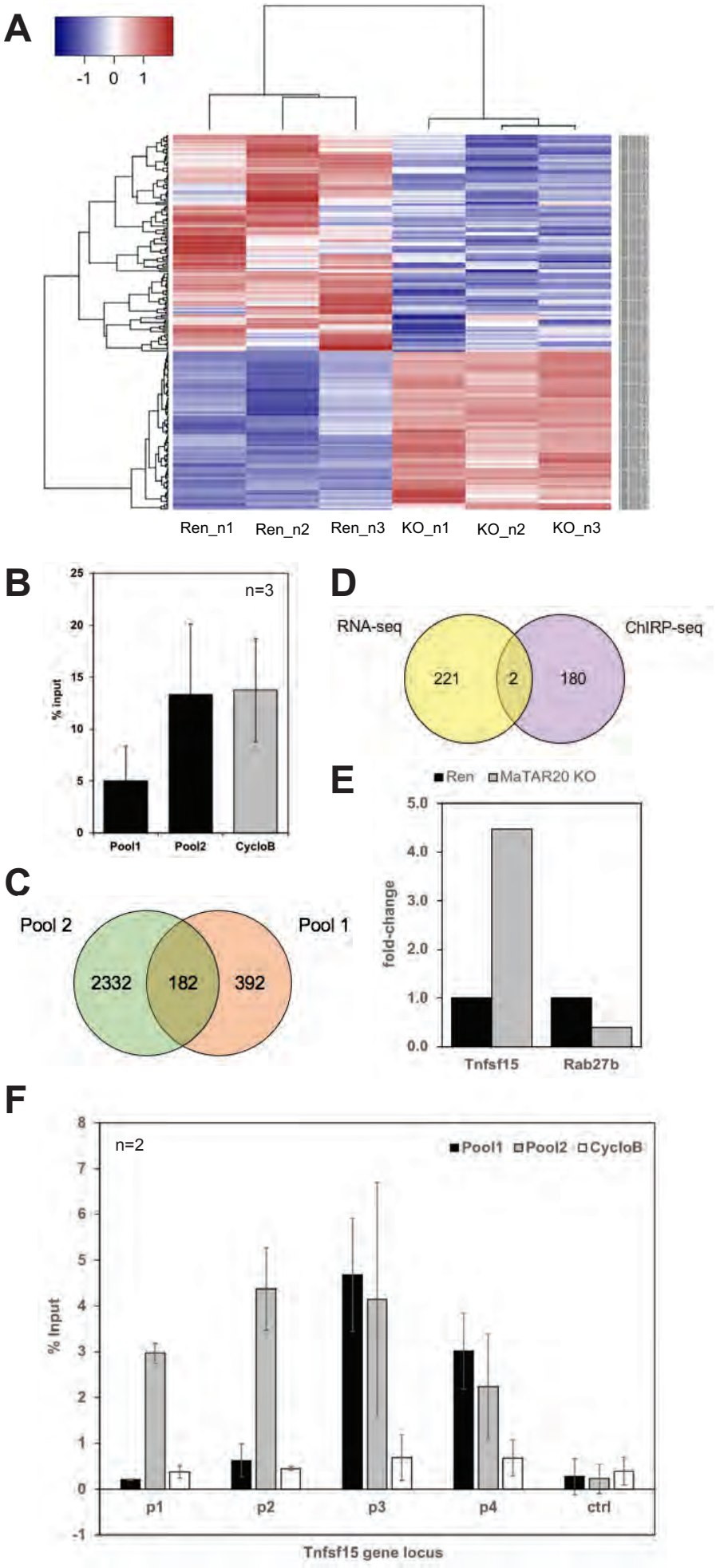
A
-1 0 1
Ren_n1
Ren_n2
Ren_n3
KO_n1
KO_n2
KO_n3
B
n=3
% input
Pool1
Pool2
CycloB
C
Pool 2
Pool 1
2332
182
392
D
RNA-seq
ChIRP-seq
221
2
180
E
Ren
MaTAR20 KO
fold-change
Tnfsf15
Rab27b
F
n=2
Pool1
Pool2
CycloB
% Input
p1
p2
p3
p4
ctrl
Tnfsf15 gene locus

Figure 7

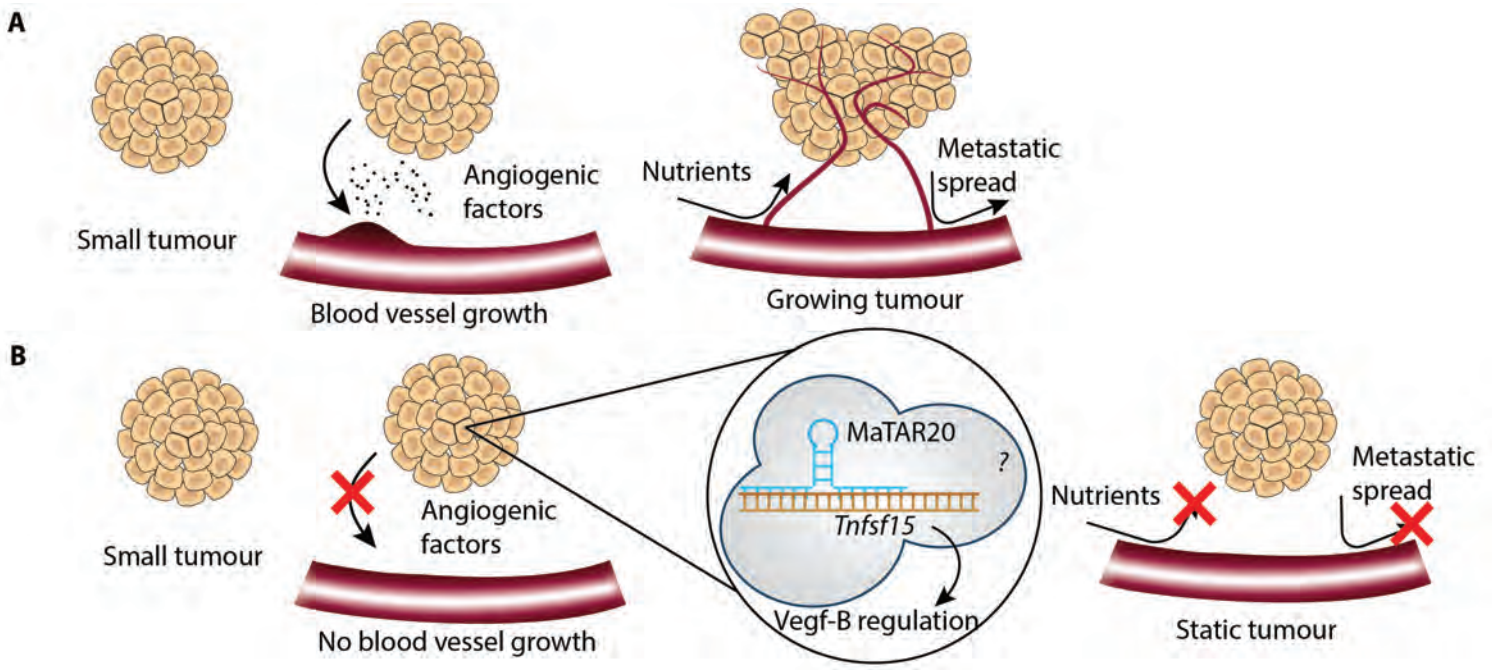
A
Small tumour
Angiogenic factors
Blood vessel growth
Nutrients
Metastatic spread
Growing tumour
B
Small tumour
Angiogenic factors
No blood vessel growth
MaTAR20
?
Tnfsf15
Vegf-B regulation
Nutrients
Metastatic spread
Static tumour

Figure 8

A

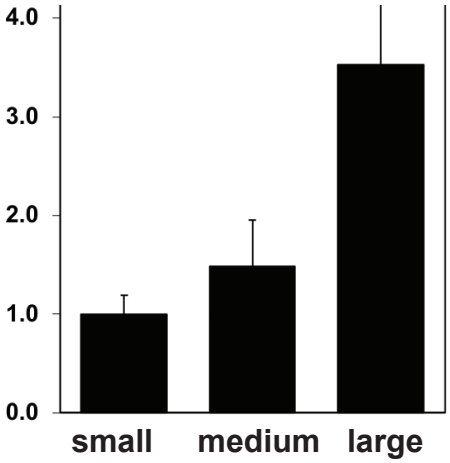


Figure S1

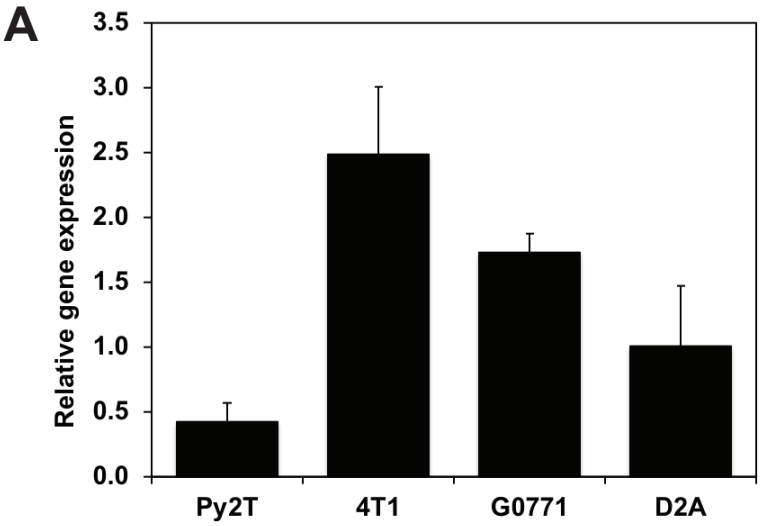
A
Relative gene expression
3.5
3.0
2.5
2.0
1.5
1.0
0.5
0.0
Py2T
4T1
G0771
D2A

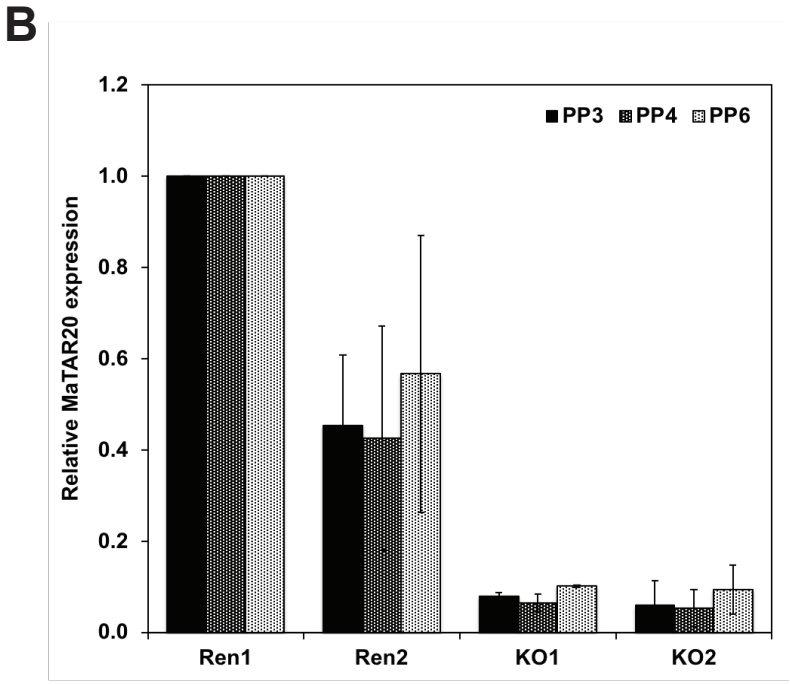
B
Relative MaTAR20 expression
PP3
PP4
PP6
1.2
1.0
0.8
0.6
0.4
0.2
0.0
Ren1
Ren2
KO1
KO2

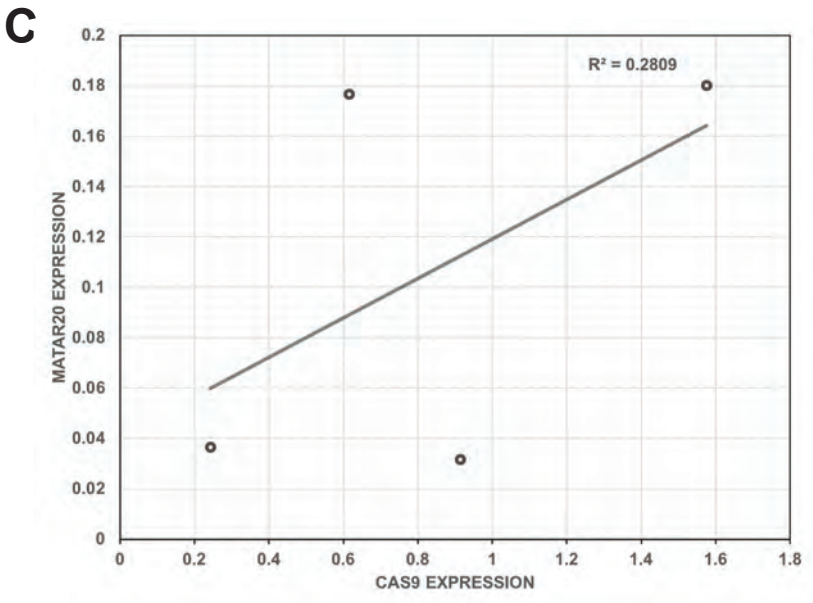
C
R² = 0.2809
MATAR20 EXPRESSION
CAS9 EXPRESSION
0.2
0.18
0.16
0.14
0.12
0.1
0.08
0.06
0.04
0.02
0
0
0.2
0.4
0.6
0.8
1
1.2
1.4
1.6
1.8

Figure S2

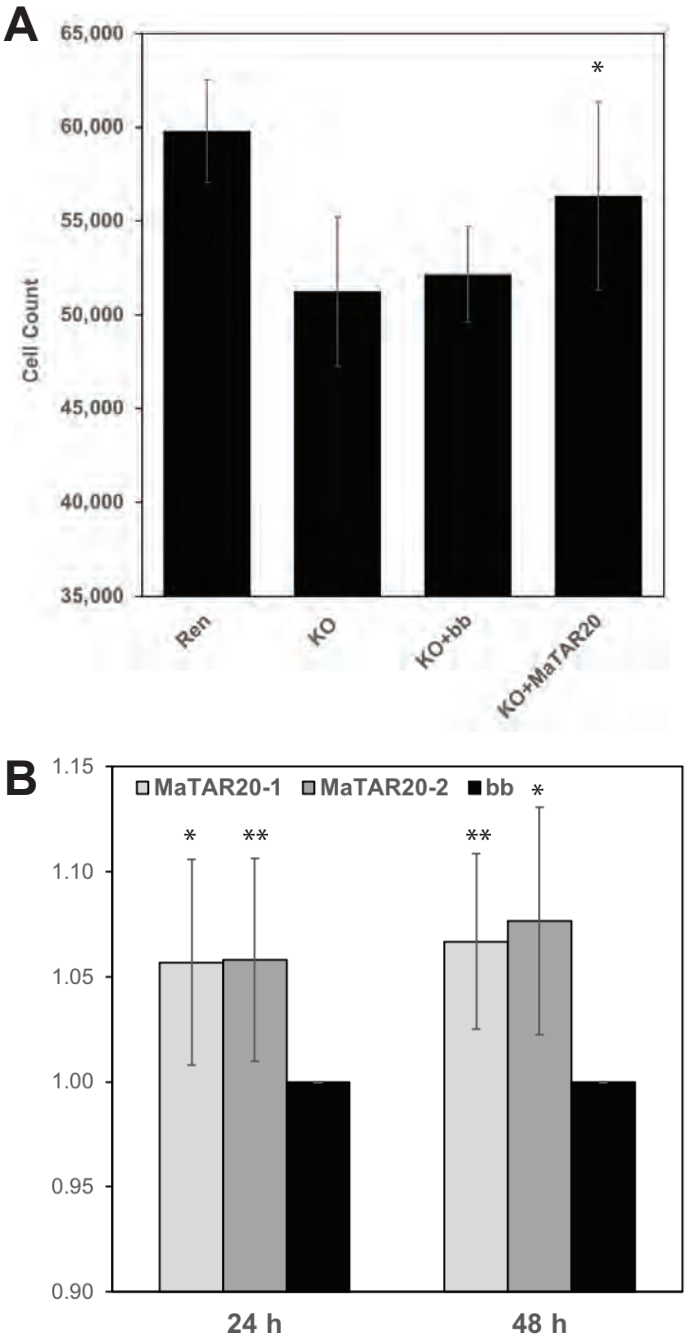
A
65,000
60,000
55,000
50,000
45,000
40,000
35,000
Cell Count
*
Ren
KO
KO+bb
KO+MaTAR20
B
1.15
1.10
1.05
1.00
0.95
0.90
MaTAR20-1
MaTAR20-2
bb
*
**
**
*
24 h
48 h

Figure S3

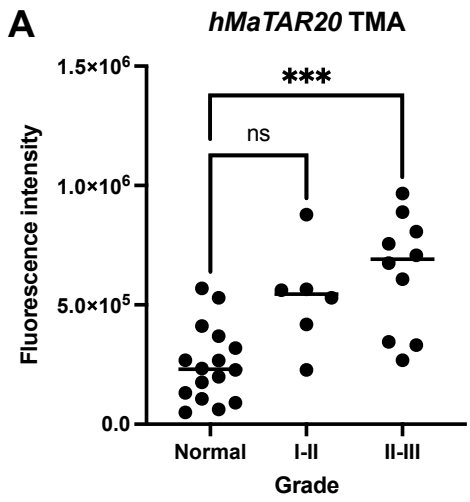
A
hMaTAR20 TMA
Fluorescence intensity
1.5×10^6
1.0×10^6
5.0×10^5
0.0
***
ns
Normal
I-II
II-III
Grade

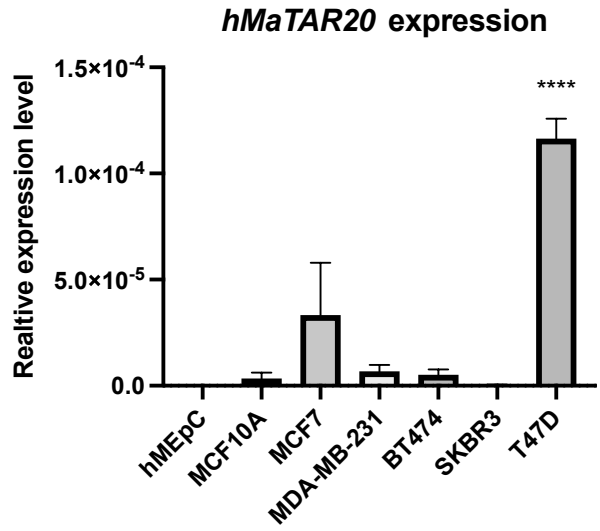
B
hMaTAR20 expression
Realtive expression level
1.5×10^-4
1.0×10^-4
5.0×10^-5
0.0
****
hMEpC
MCF10A
MCF7
MDA-MB-231
BT474
SKBR3
T47D

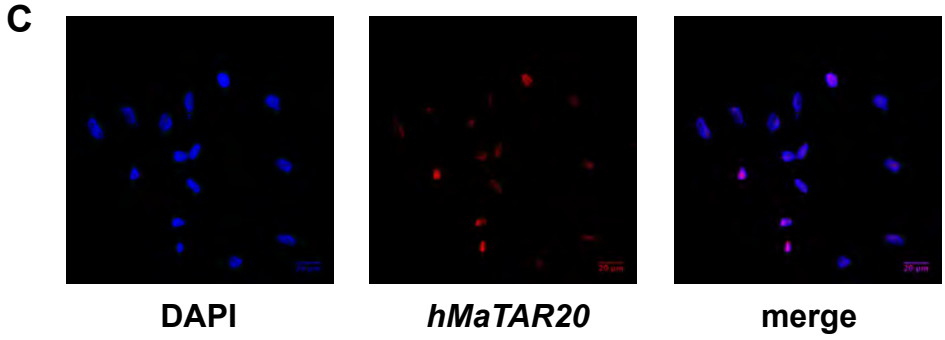
C
DAPI
hMaTAR20
merge

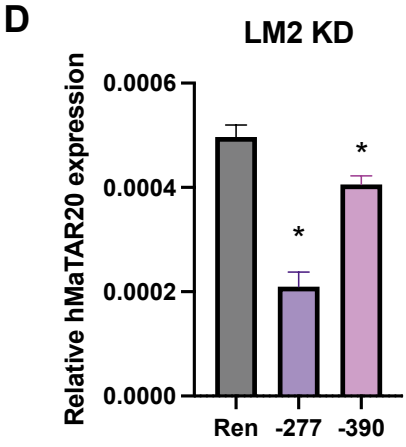
D
LM2 KD
Relative hMaTAR20 expression
0.0006
0.0004
0.0002
0.0000
*
*
Ren
-277
-390

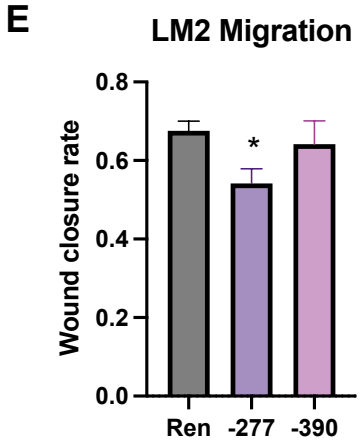
E
LM2 Migration
Wound closure rate
0.8
0.6
0.4
0.2
0.0
*
Ren
-277
-390

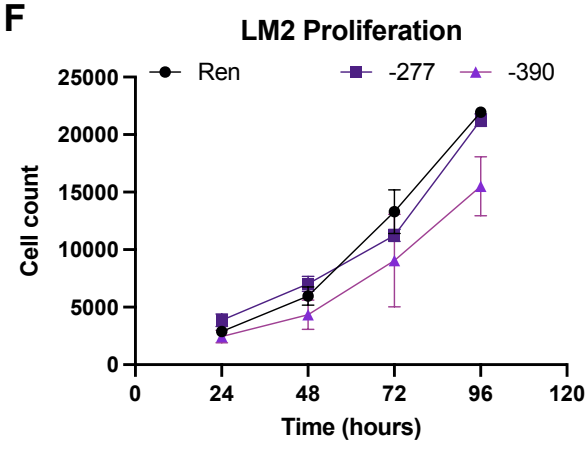
F
LM2 Proliferation
Ren
-277
-390
Cell count
25000
20000
15000
10000
5000
0
0
24
48
72
96
120
Time (hours)

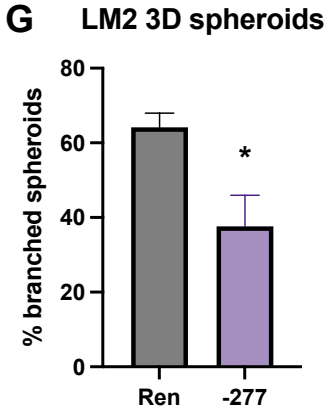
G
LM2 3D spheroids
% branched spheroids
80
60
40
20
0
*
Ren
-277

Figure S4

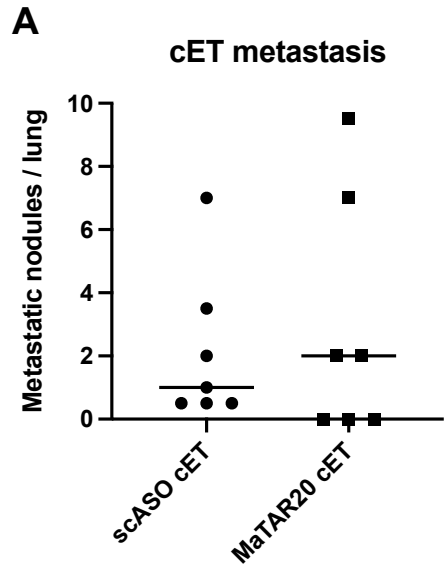
A
cET metastasis
Metastatic nodules / lung
10
8
6
4
2
0
scASO cET
MaTAR20 cET

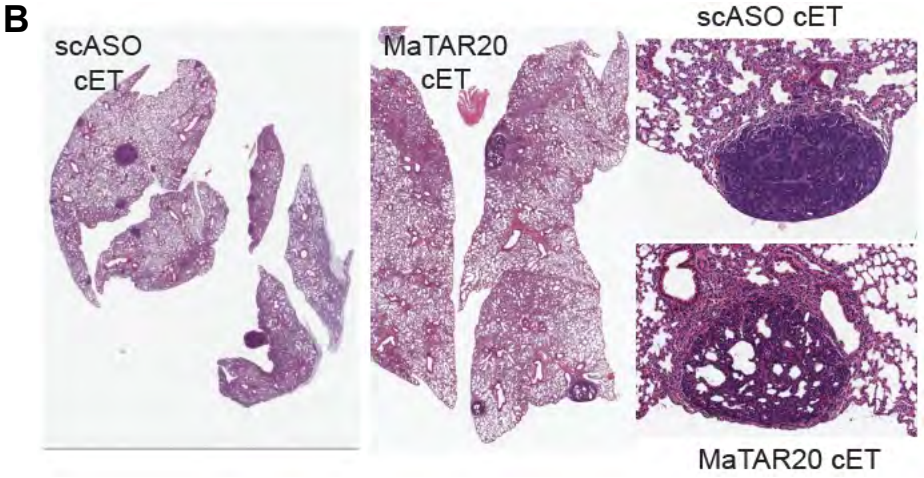
B
scASO
cET
MaTAR20
cET
scASO cET
MaTAR20 cET

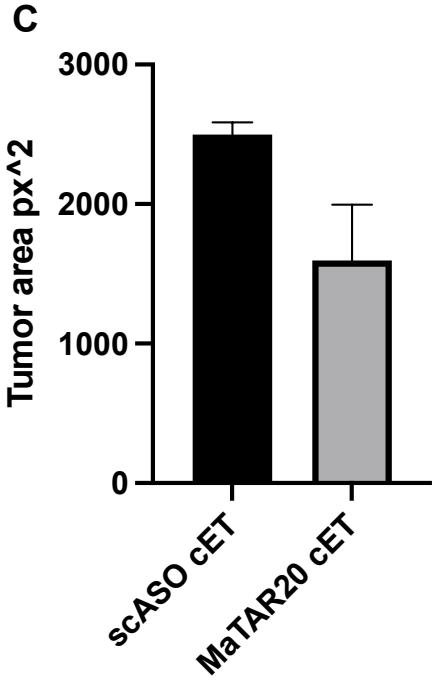
C
Tumor area px^2
3000
2000
1000
0
scASO cET
MaTAR20 cET

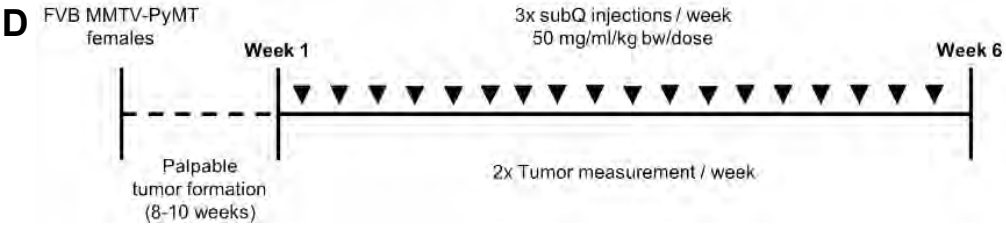
D
FVB MMTV-PyMT
females
Week 1
3x subQ injections / week
50 mg/ml/kg bw/dose
Week 6
Palpable
tumor formation
(8-10 weeks)
2x Tumor measurement / week

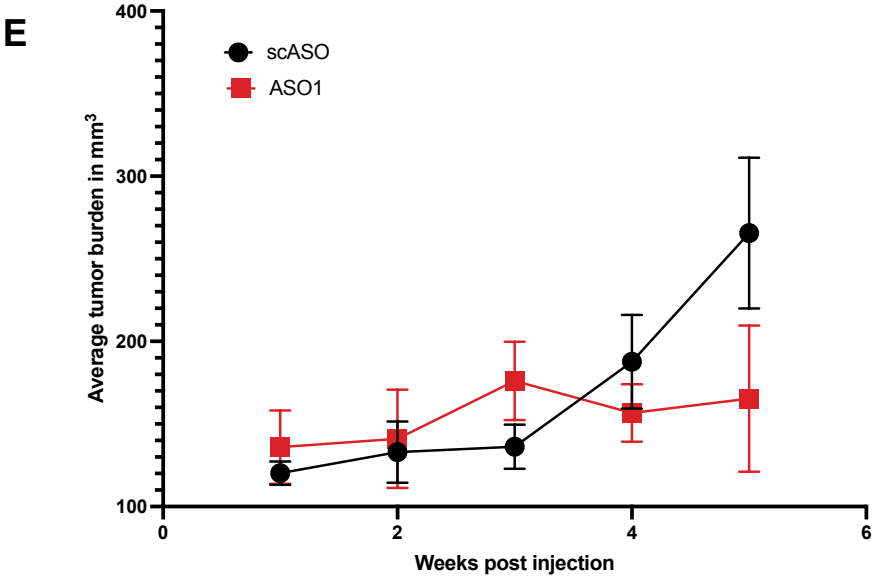
E
scASO
ASO1
Average tumor burden in mm3
400
300
200
100
0
2
4
6
Weeks post injection

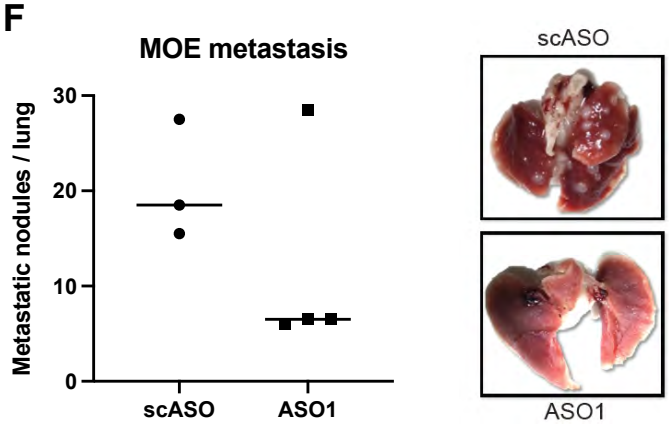
F
MOE metastasis
Metastatic nodules / lung
30
20
10
0
scASO
ASO1
scASO
ASO1

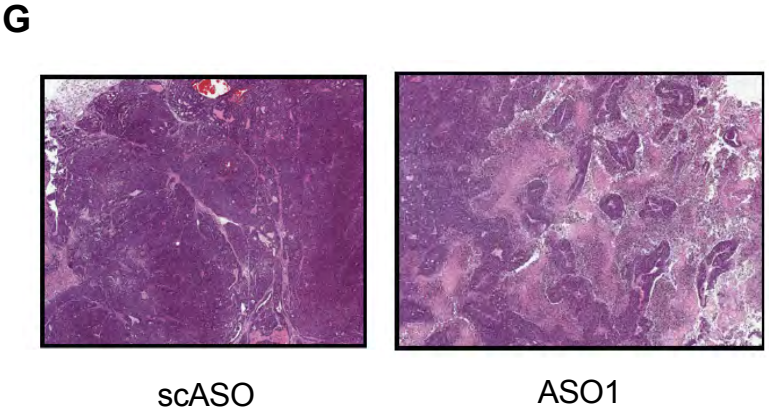
G
scASO
ASO1

**Figure S5**

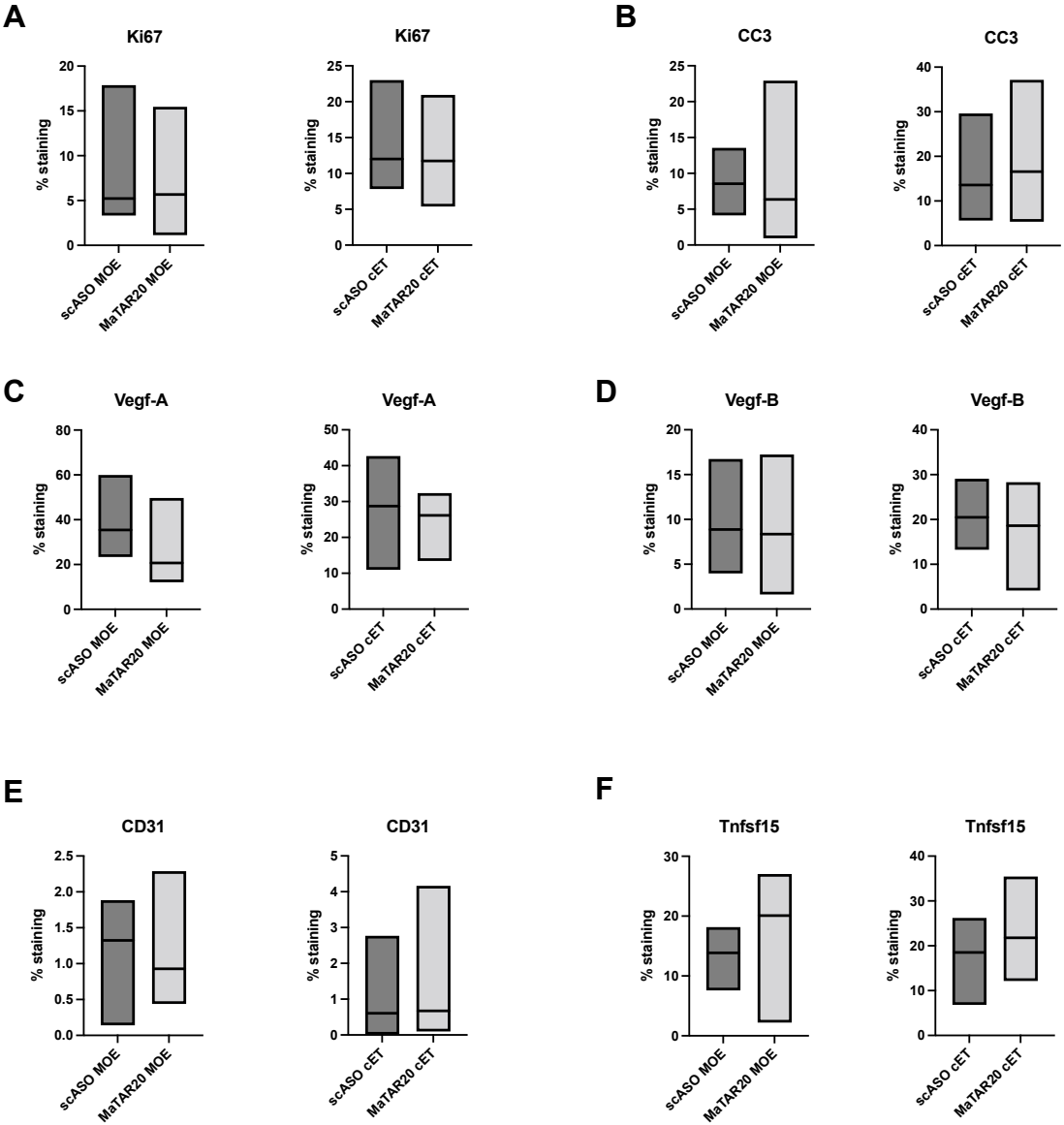
A
Ki67
% staining
scASO MOE
MaTAR20 MOE
Ki67
% staining
scASO cET
MaTAR20 cET
B
CC3
% staining
scASO MOE
MaTAR20 MOE
CC3
% staining
scASO cET
MaTAR20 cET
C
Vegf-A
% staining
scASO MOE
MaTAR20 MOE
Vegf-A
% staining
scASO cET
MaTAR20 cET
D
Vegf-B
% staining
scASO MOE
MaTAR20 MOE
Vegf-B
% staining
scASO cET
MaTAR20 cET
E
CD31
% staining
scASO MOE
MaTAR20 MOE
CD31
% staining
scASO cET
MaTAR20 cET
F
Tnfsf15
% staining
scASO MOE
MaTAR20 MOE
Tnfsf15
% staining
scASO cET
MaTAR20 cET

Figure S6

A

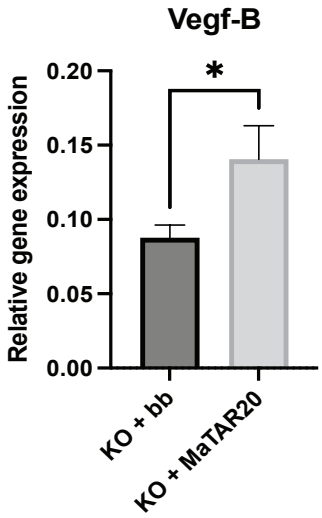


B

| Top10 up | | |
|---|---|---|
| Gene ID | log2FC | adj. p-value |
| Galm | 3.65 | 3.53E-19 |
| Gm17094 | 2.45 | 3.32E-06 |
| Pla2g5 | 2.41 | 5.21E-06 |
| Slc9a7 | 2.18 | 7.06E-05 |
| Ank2 | 2.17 | 1.57E-06 |
| Vegi | 2.16 | 3.17E-05 |
| Ophn1 | 2.10 | 0.0001 |
| Prrx2 | 2.07 | 0.0002 |
| Zswim5 | 2.00 | 1.30E-06 |
| Gm6526 | 1.95 | 0.0010 |

| Top10 down | | |
|---|---|---|
| Gene ID | log2FC | adj. p-value |
| Zfp518a | -4.67 | 1.63E-34 |
| Cobl | -4.31 | 2.21E-26 |
| Sh3tc2 | -4.06 | 1.07E-19 |
| Mall | -3.44 | 1.00E-16 |
| Sirpa | -2.83 | 9.58E-12 |
| Calhm2 | -2.78 | 6.22E-11 |
| Ccdc122 | -2.75 | 4.49E-12 |
| Eva1b | -2.72 | 4.35E-09 |
| Apc2 | -2.62 | 4.21E-08 |
| Sowahb | -2.51 | 1.84E-09 |

C

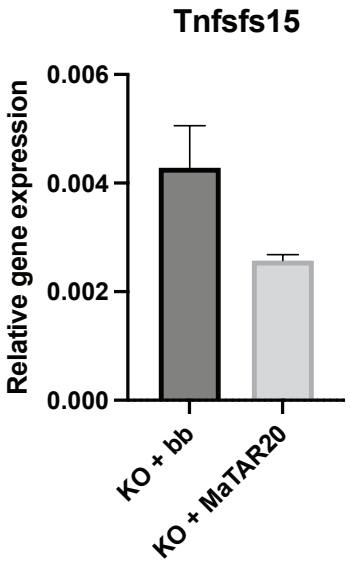


D

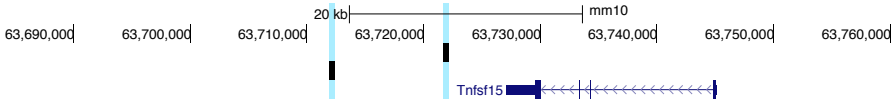


Figure S7

A

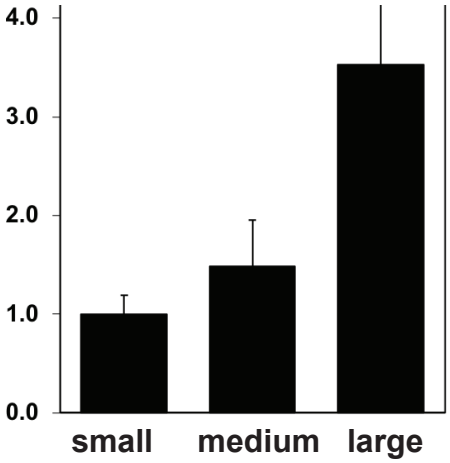


Figure S1

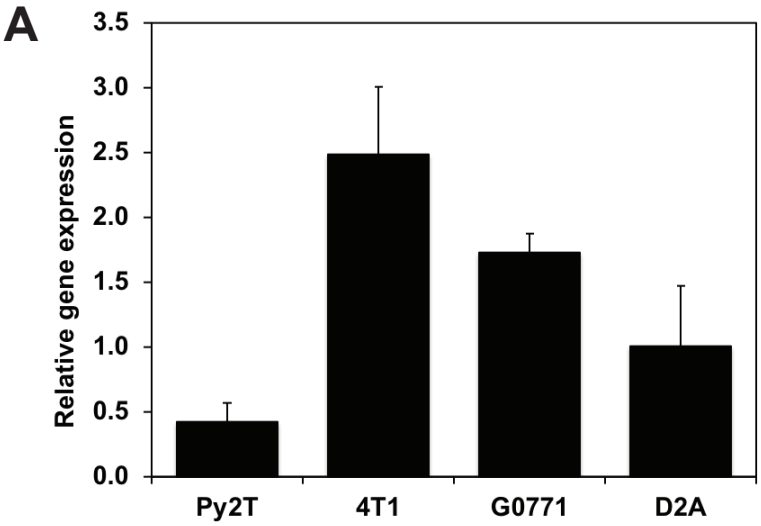
A
Relative gene expression
3.5
3.0
2.5
2.0
1.5
1.0
0.5
0.0
Py2T
4T1
G0771
D2A

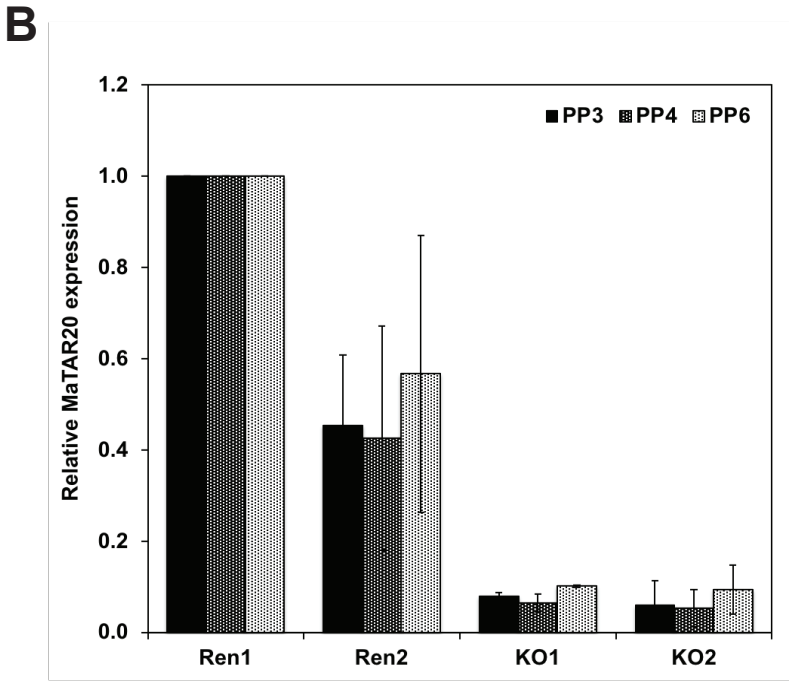
B
Relative MaTAR20 expression
PP3
PP4
PP6
1.2
1.0
0.8
0.6
0.4
0.2
0.0
Ren1
Ren2
KO1
KO2

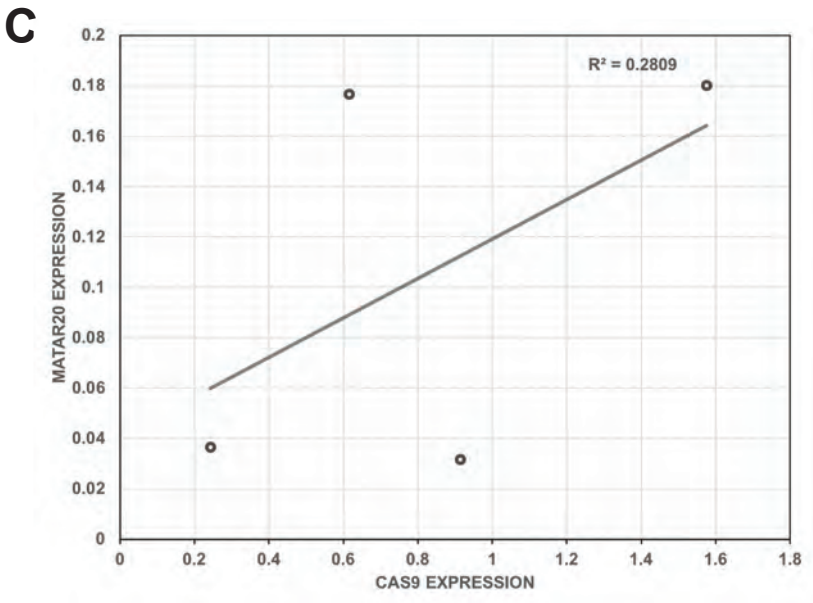
C
R² = 0.2809
MATAR20 EXPRESSION
CAS9 EXPRESSION
0.2
0.18
0.16
0.14
0.12
0.1
0.08
0.06
0.04
0.02
0
0
0.2
0.4
0.6
0.8
1
1.2
1.4
1.6
1.8

Figure S2

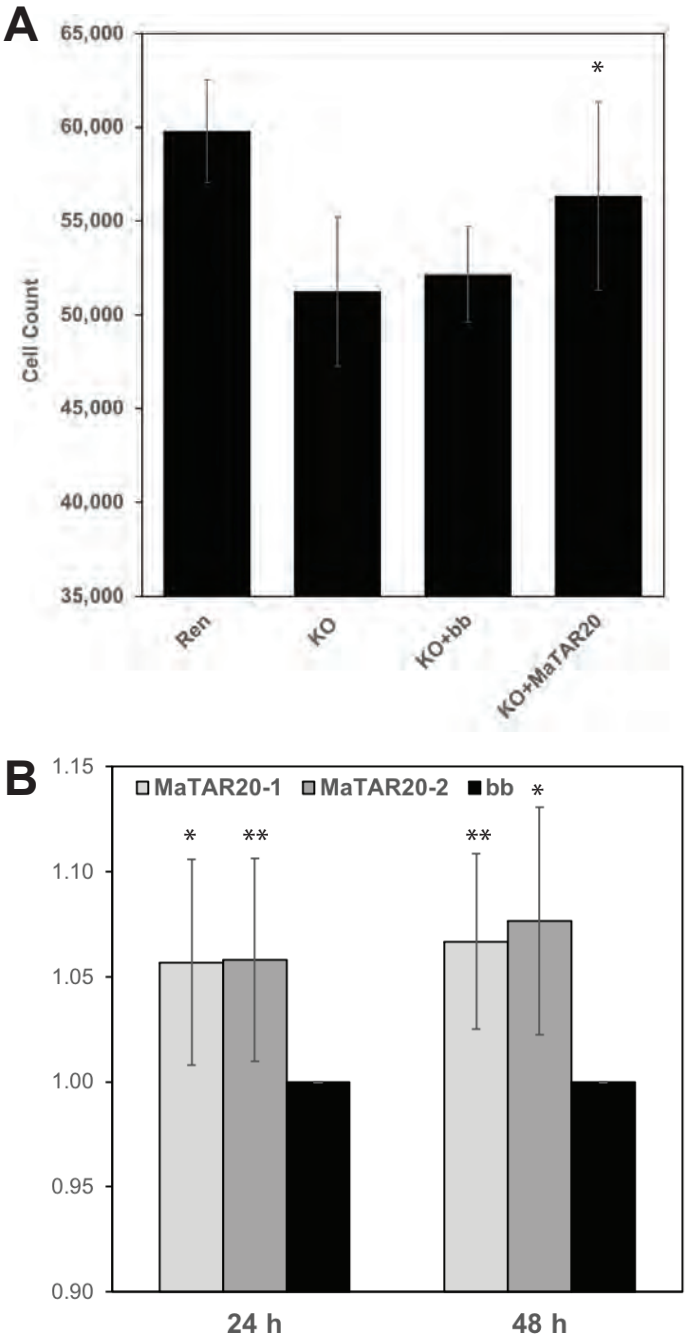
A
65,000
60,000
55,000
50,000
45,000
40,000
35,000
Cell Count
*
Ren
KO
KO+bb
KO+MaTAR20
B
1.15
1.10
1.05
1.00
0.95
0.90
MaTAR20-1
MaTAR20-2
bb
*
**
**
*
24 h
48 h

Figure S3

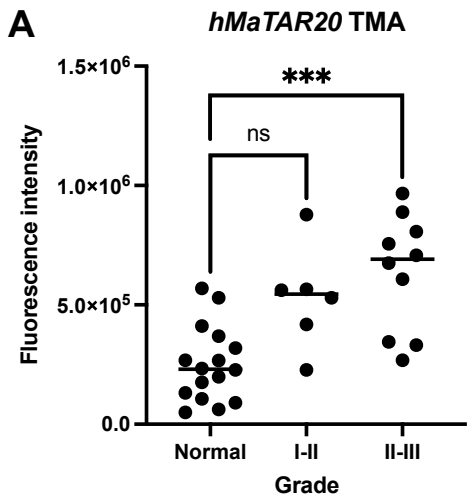
A
hMaTAR20 TMA
Fluorescence intensity
1.5×10^6
1.0×10^6
5.0×10^5
0.0
***
ns
Normal
I-II
II-III
Grade

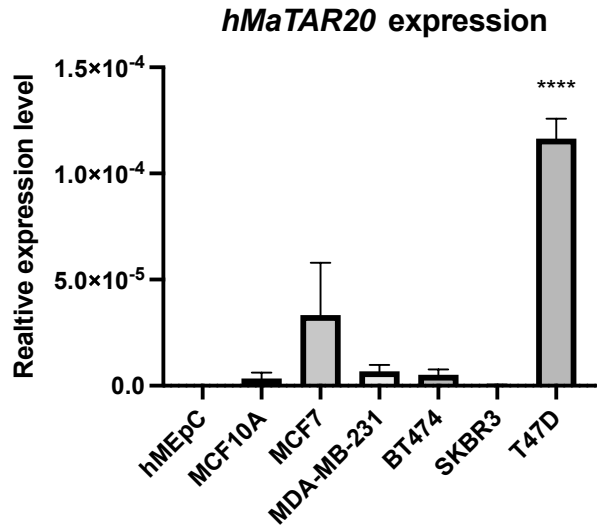
B
hMaTAR20 expression
Realtive expression level
1.5×10^-4
1.0×10^-4
5.0×10^-5
0.0
****
hMEpC
MCF10A
MCF7
MDA-MB-231
BT474
SKBR3
T47D

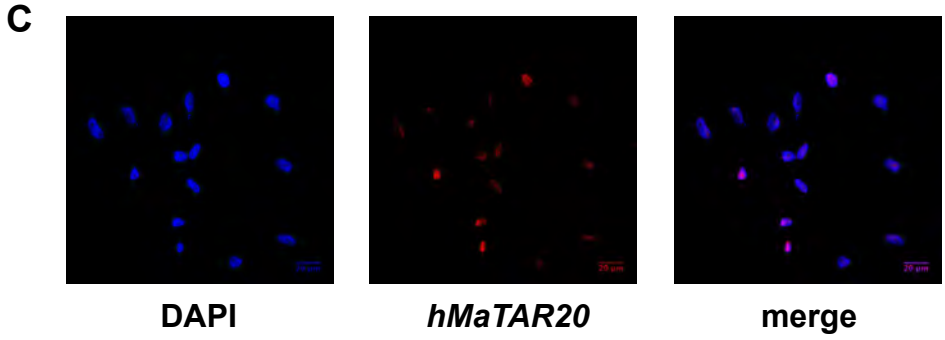
C
DAPI
hMaTAR20
merge

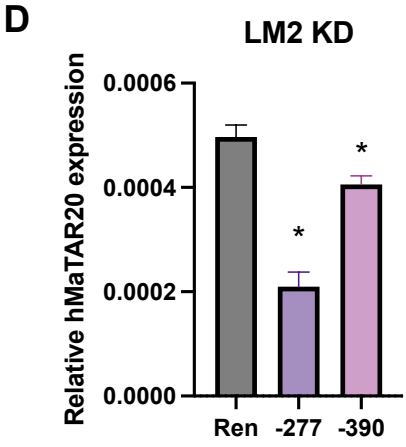
D
LM2 KD
Relative hMaTAR20 expression
0.0006
0.0004
0.0002
0.0000
*
*
Ren
-277
-390

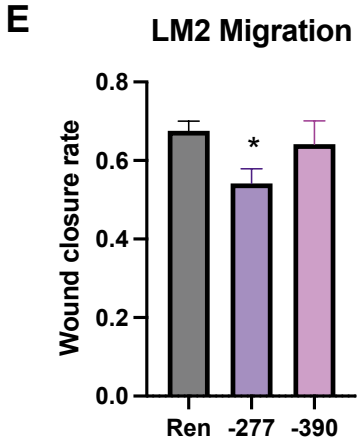
E
LM2 Migration
Wound closure rate
0.8
0.6
0.4
0.2
0.0
*
Ren
-277
-390

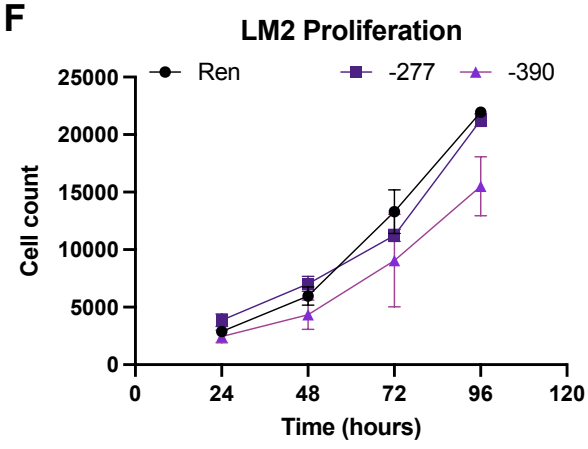
F
LM2 Proliferation
Ren
-277
-390
Cell count
25000
20000
15000
10000
5000
0
0
24
48
72
96
120
Time (hours)

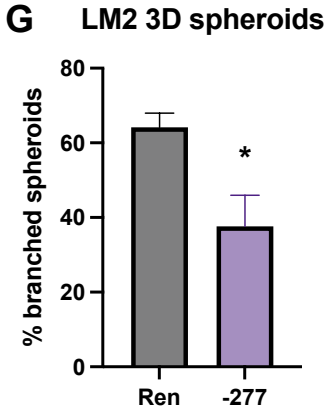
G
LM2 3D spheroids
% branched spheroids
80
60
40
20
0
*
Ren
-277

Figure S4

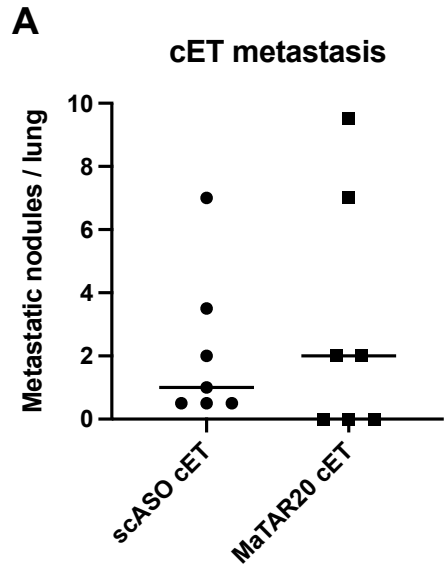
A
cET metastasis
Metastatic nodules / lung
10
8
6
4
2
0
scASO cET
MaTAR20 cET

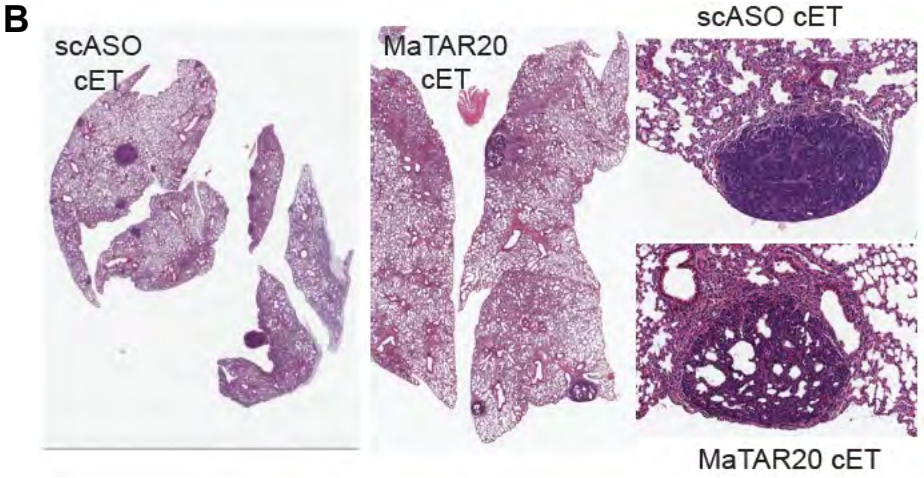
B
scASO
cET
MaTAR20
cET
scASO cET
MaTAR20 cET

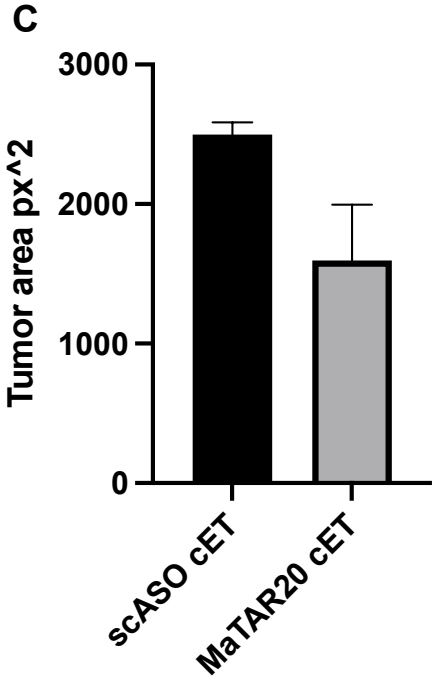
C
Tumor area px^2
3000
2000
1000
0
scASO cET
MaTAR20 cET

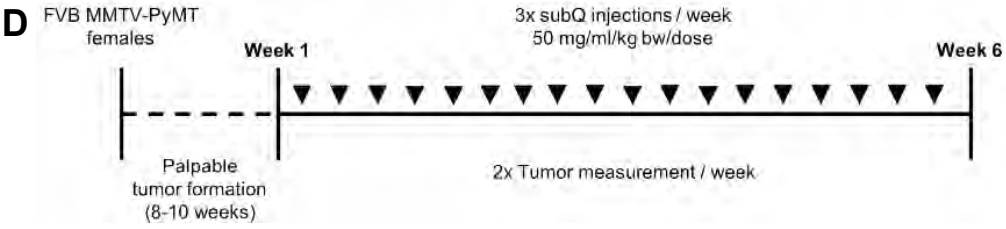
D
FVB MMTV-PyMT
females
Week 1
3x subQ injections / week
50 mg/ml/kg bw/dose
Week 6
Palpable
tumor formation
(8-10 weeks)
2x Tumor measurement / week

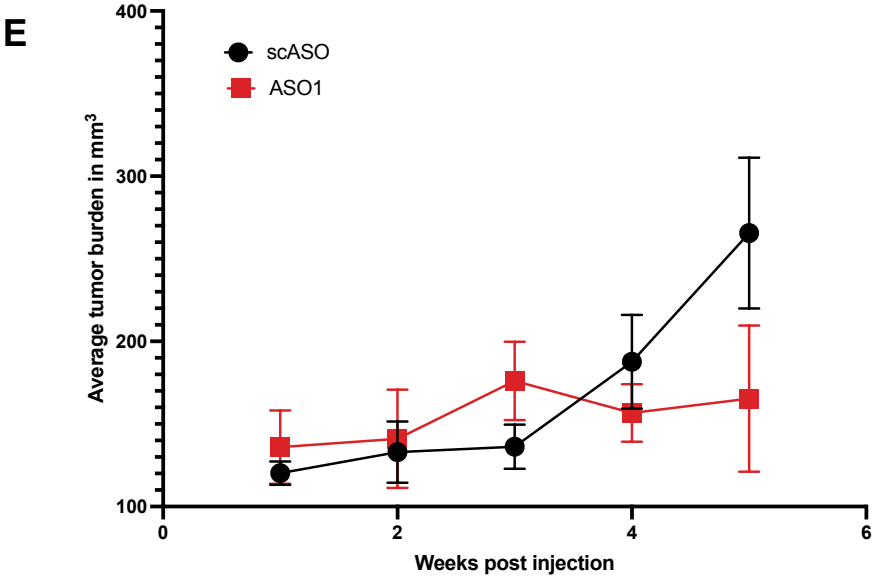
E
scASO
ASO1
Average tumor burden in mm3
400
300
200
100
0
2
4
6
Weeks post injection

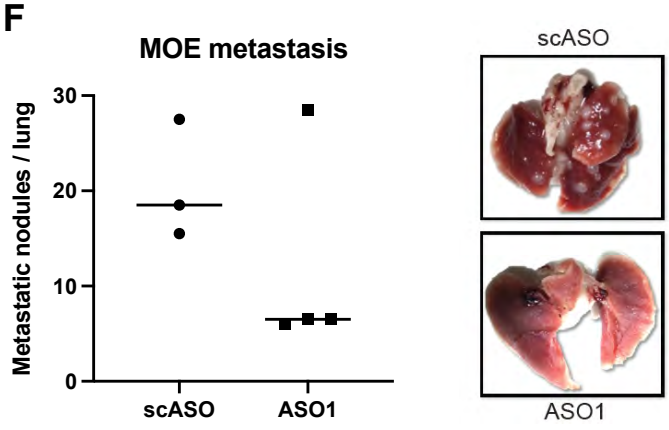
F
MOE metastasis
Metastatic nodules / lung
30
20
10
0
scASO
ASO1
scASO
ASO1

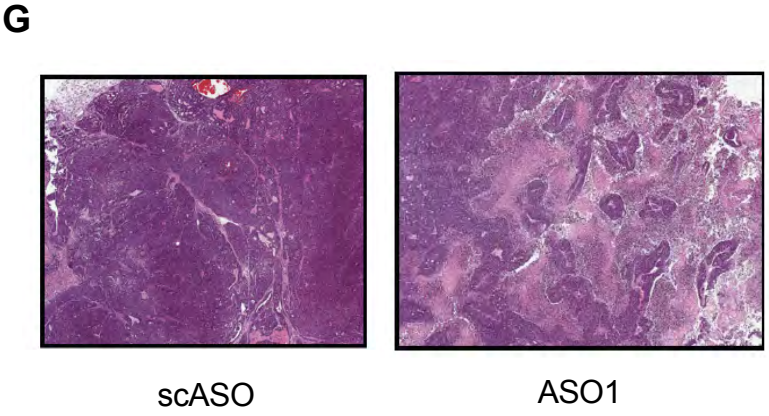
G
scASO
ASO1

**Figure S5**

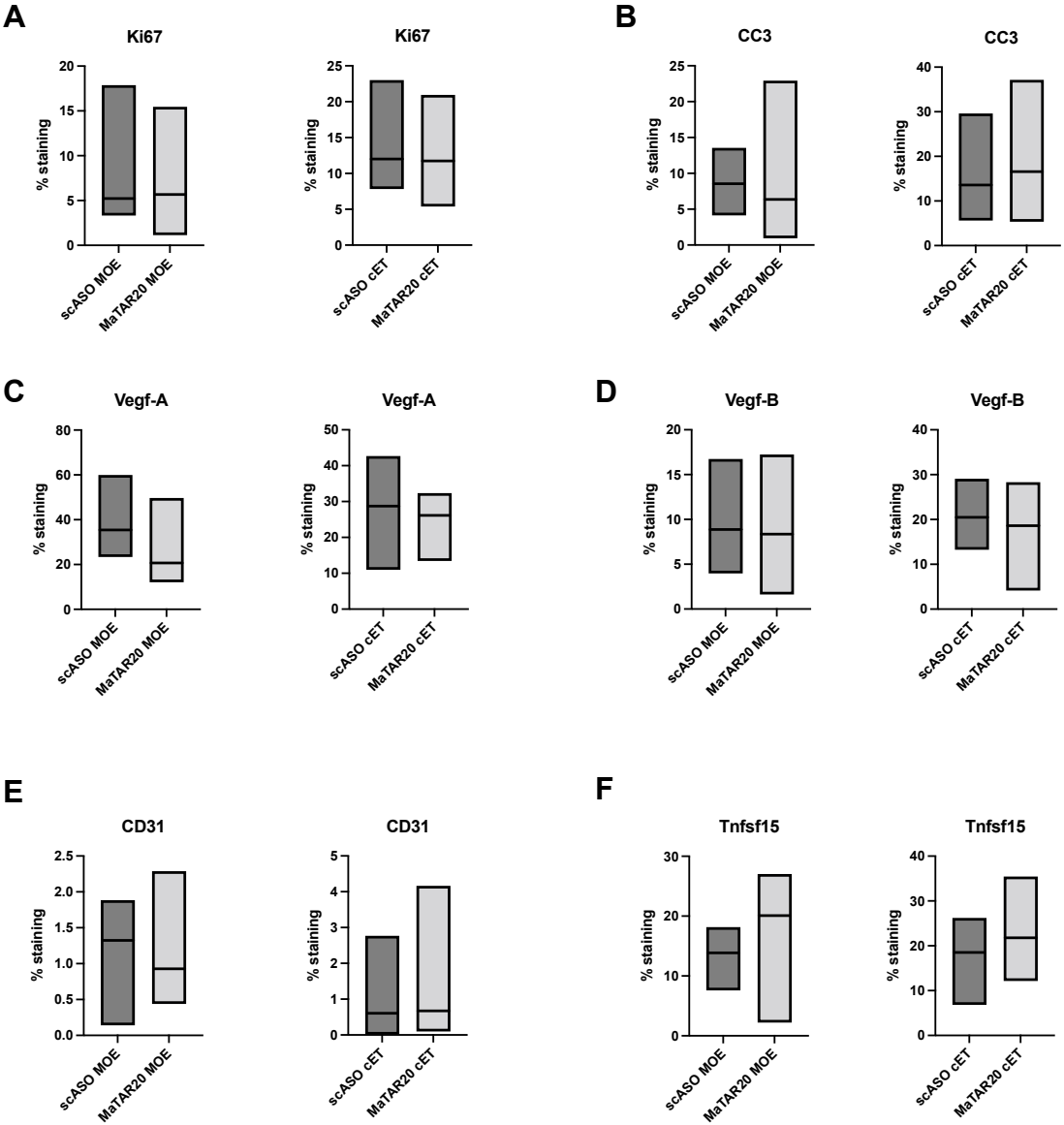
A
Ki67
% staining
scASO MOE
MaTAR20 MOE
Ki67
% staining
scASO cET
MaTAR20 cET
B
CC3
% staining
scASO MOE
MaTAR20 MOE
CC3
% staining
scASO cET
MaTAR20 cET
C
Vegf-A
% staining
scASO MOE
MaTAR20 MOE
Vegf-A
% staining
scASO cET
MaTAR20 cET
D
Vegf-B
% staining
scASO MOE
MaTAR20 MOE
Vegf-B
% staining
scASO cET
MaTAR20 cET
E
CD31
% staining
scASO MOE
MaTAR20 MOE
CD31
% staining
scASO cET
MaTAR20 cET
F
Tnfsf15
% staining
scASO MOE
MaTAR20 MOE
Tnfsf15
% staining
scASO cET
MaTAR20 cET

Figure S6

A

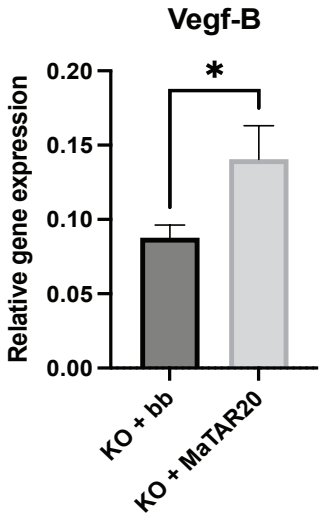


B

| Top10 up | | |
|---|---|---|
| Gene ID | log2FC | adj. p-value |
| Galm | 3.65 | 3.53E-19 |
| Gm17094 | 2.45 | 3.32E-06 |
| Pla2g5 | 2.41 | 5.21E-06 |
| Slc9a7 | 2.18 | 7.06E-05 |
| Ank2 | 2.17 | 1.57E-06 |
| Vegi | 2.16 | 3.17E-05 |
| Ophn1 | 2.10 | 0.0001 |
| Prrx2 | 2.07 | 0.0002 |
| Zswim5 | 2.00 | 1.30E-06 |
| Gm6526 | 1.95 | 0.0010 |

| Top10 down | | |
|---|---|---|
| Gene ID | log2FC | adj. p-value |
| Zfp518a | -4.67 | 1.63E-34 |
| Cobl | -4.31 | 2.21E-26 |
| Sh3tc2 | -4.06 | 1.07E-19 |
| Mall | -3.44 | 1.00E-16 |
| Sirpa | -2.83 | 9.58E-12 |
| Calhm2 | -2.78 | 6.22E-11 |
| Ccdc122 | -2.75 | 4.49E-12 |
| Eva1b | -2.72 | 4.35E-09 |
| Apc2 | -2.62 | 4.21E-08 |
| Sowahb | -2.51 | 1.84E-09 |

C

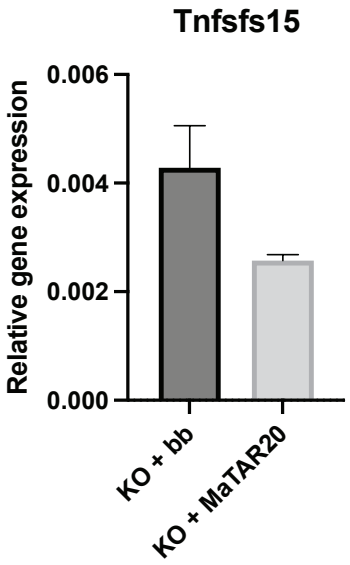


D

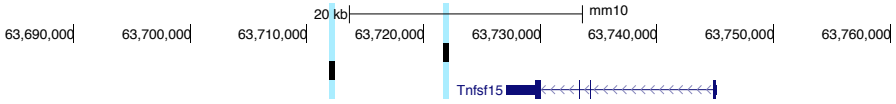


Figure S7